Journal of Reliability Science and Engineering

Time-variant system reliability analysis via stochastic process discretization and most probable point trajectory approximation

OPEN ACCESS
IOP Publishing | ISECAEP
Journal of Reliability Science and Engineering
J. Reliab. Sci. Eng. **1** (2025) 025001 (21pp)
https://doi.org/10.1088/3050-2454/adc45d

Time-variant system reliability analysis via stochastic process discretization and most probable point trajectory approximation

Dequan Zhang, Hongfei Zhang, Pengfei Zhou, Xing-ao Li, Fang Wang and Xu Han*

State Key Laboratory of Intelligent Power Distribution Equipment and System, School of Mechanical Engineering, Hebei University of Technology, 300401 Tianjin, People's Republic of China

E-mail: xhan@hebut.edu.cn

Received 15 January 2025, revised 24 February 2025
Accepted for publication 20 March 2025
Published 10 April 2025

Abstract

Time-variant reliability analysis for single failure mode has advanced considerably and now exhibits great potential. However, in practical engineering applications, structures and systems generally invoke multiple failure modes. This poses a lasting challenge for current reliability analysis and simultaneously entails very high, if not intractable, computational cost. Therefore, developing an accurate time-variant system reliability model that accounts for multiple failure modes and its commensurate solution strategy is imperative. To this objective, this study develops an innovative method to assess time-variant system reliability by utilizing the Kriging model. First, multiple failure modes are decomposed into separate time-variant reliability assessments, each addressing a single failure mode. Inspired by the discretization of stochastic processes, each time-variant function in the structural system is assumed to be a set of time-invariant reliability problems. Subsequently, for each time-invariant reliability issue, the most probable point (MPP) is determined and the performance function is linearized and expanded accordingly. On this basis, the Kriging model of the MPP at discrete time is constructed. To enhance the model's precision, an active learning technique is employed for ongoing model updates. Finally, the reliability index and failure probability are determined by solving time-invariant system reliability models. The proposed method s applicability and effectiveness are demonstrated through exemplifications of variable systems.

Keywords: time-variant reliability analysis, multiple failure modes, Kriging model, active learning, MPP trajectory approximation

* Author to whom any correspondence should be addressed.

Nomenclature

a	The order units in series system.
b	The order units in parallel system.
$B_{i,j}$	The reliable events of functional units.
$\mathbf{C}_{\boldsymbol{\alpha}_j}$	The correlation coefficient matrix of $\boldsymbol{\alpha}_j$.
E	The reliability event.
$F_{Q_{i,j}}(\cdot)$	The distribution function of $Q_{i,j}$.
$g(\cdot)$	The performance function of the structure.
$\hat{g}(\cdot)$	The prediction of the Kriging model.
$\breve{g}_j(\cdot)$	The performance function under variables $\mathbf{V}$ and Q_j.
$G'(\cdot)$	The partial derivatives of performance function at the MPP.
$\breve{G}_i(\cdot)$	The performance function $\breve{g}_j(\cdot)$ in standard normal space.
$G_{i,k}(\cdot)$	The performance function of the parallel system.
$G_{j,k}(\cdot)$	The performance function of the series system.
$G_{i,j,k}(\cdot)$	The performance function of the mixed system.
p	The number of time interval Δt.
$P_{\mathrm{s}}(\cdot)$	The failure probability of the structure.
$Q_{i,j}$	The transition variable.
$R(\cdot,\cdot)$	The correlation coefficient of two sample.
t^*	The point added to the training set through the U function.
t_k	The kth discrete time point.
$\mathbf{U}$	Random variable in the standard normal space.
U'_k	The mean of random variable of the kth performance function.
$U''_{i,j,k}$	The random variable of the MPP of $G_{i,j,k}(\mathbf{V},\mathbf{U}_k,t_k)$.
$\mathbf{V}$	Stochastic processes in standard normal space.
V'	The mean of the stochastic process.
$V''_{i,j,k}$	The stochastic process of the MPP of $G_{i,j,k}(\mathbf{V},\mathbf{U}_k,t_k)$.
$\mathbf{X}$	The random variable.
$\mathbf{Y}$	The stochastic process.
$\mathbf{Z}_j$	The variable consisting of $\mathbf{V}$ and Q_j.
$\mathbf{Z'}_i^*$	The MPP of performance function $\breve{G}_i(\mathbf{Z'}_i)$.
$\mathbf{Z}_{\mathrm{MPP}(t_k)}^{(i,j)}$	The MPP of the performance function $G_{i,j,k}$ at t_k.
$\hat{\mathbf{Z}}_{\mathrm{MPP}}^{(i,j,k)}(\cdot)$	Prediction of the MPP at t_k through the Kriging model.
$\boldsymbol{\alpha}_j$	The transition variable.
β_{r}	The reliability index.
$\boldsymbol{\mu}_{\boldsymbol{\alpha}_j}$	The mean of $\boldsymbol{\alpha}_j$.
$v^+(\cdot)$	The crossing rate.
$\boldsymbol{\rho}_{\mathbf{X}}$	The correlation coefficient matrix of the random variable $\mathbf{X}$.
$\boldsymbol{\rho}_{\mathbf{Y}}$	The correlation coefficient matrix of the stochastic process $\mathbf{Y}$.
$\hat{\sigma}^2_{\hat{g}(\mathbf{X})}$	The prediction variance of the Kriging model.
$\hat{\boldsymbol{\sigma}}_{\hat{\mathbf{Z}}_{\mathrm{MPP}}^{(i,j,k)}}(\cdot)$	Predicted variance of the MPP at t_k through the Kriging model.
$\mathrm{Cov}(\cdot,\cdot)$	The covariance matrix between different failure modes.

1. Introduction

In practical engineering applications, system reliability, due to the impact of random dynamic loads, material degradation, and other time-variant factors [1], inevitably changes over time instead of staying constant. Therefore, conducting a time-variant reliability analysis throughout the entire lifetime of a structure/system is of paramount importance [1]. However, accounting for this variability significantly increases both the complexity and computational cost of the analysis. This is due to the stochastic variation of system parameters over time, the intricacy in dynamic behaviors, and the prerequisite for high accuracy in probabilistic calculations [2, 3]. To enhance computational efficiency, numerous time-variant reliability analysis methods have been proposed. These methods can basically be categorized into three types [4]: (1) outcrossing rate-based methods, which calculate time-variant reliability based on a diplomatic rate of structural performance; (2) composite limit state methods, which transform the time-variant reliability analysis into time-independent analysis by discretizing both the time intervals and stochastic processes; and (3) surrogate model-based methods, which construct surrogate models to approximate actual performance function.

The outcrossing method [5] is widely used to tackle time-variant reliability problems. To start with, the outcrossing method calculates the outcrossing of the structural performance function at each specific time instant. Assumptions, such as the Poisson process hypothesis [6], the Markov process hypothesis [7] or their enhanced models [8], are usually made to convert the outcrossing data into reliability estimates. Specifically, Rice [9, 10] investigated the crossover behavior between time-variant responses and their permissible limits, introducing the well-known Rice formula. This work lays the groundwork for the notion of first crossover failure. Engelund *et al* [11] introduced an approximation via high-order threshold crossing for the first crossing time of differentiable processes. Schall *et al* [12] and Rackwitz [13] employed this method to address dynamic loads in time-variant issues. Zhang and Du [14] further applied this model to structural reliability mechanism analysis. Andrieu-Renaud *et al* [5] introduced the PHI2 method in combination with the first-order reliability method (FORM) [15] to analyze the crossover rate. This approach streamlined the assessment of time-variant reliability and enhanced computational efficiency. Sudret [16] advanced the PHI2 method into the PHI2+ approach, which exhibited improved stability compared to its original version. Singh *et al* [17, 18] applied the importance sampling technique to compute the span rate in time-variant reliability analysis, which effectively tackled minor failure probability problems. Hu *et al* [19] converted the performance function into a Gaussian process and applied the Rice formula to compute the failure probability at various time instants.

Unlike the outcrossing rate-based method, the composite limit state method first discretizes the time-variant performance function into a series of time-independent performance functions. These time-invariant performance functions are then assessed using classical reliability analysis techniques, and the time-variant reliability is derived by analyzing their interdependencies. Jiang *et al* [20, 21] proposed a time-variant reliability analysis method based on stochastic process discretization (TRPD), followed by an improved version of the TRPD method that further simplified the solution process compared to the original approach. However, as the number of discrete stochastic processes and time intervals increase, the computational cost steps up exponentially [22]. In recent years, surrogate model-based methods have gained significant attention due to their potential to significantly enhance the computational efficiency and accuracy of time-variant reliability analysis [23]. By considering the correlation between time trajectories, Song *et al* [24] proposed an estimation variance reduction-guided adaptive Kriging method. Wu *et al* [25] proposed a parallel EGO method to add multiple candidate samples to the Kriging model at each iteration. Ji *et al* [26] applied adaptive downscaling and agent-based modeling to time-variant reliability analysis, effectively addressing the challenge of systems with high-dimensional inputs. Song *et al* [27] proposed a dimension reduction-based Kriging modeling method for high-dimensional time-variant uncertainty propagation and global sensitivity analysis. For time-variant reliability with small failure probability, Guo *et al* [28] presented a novel method for small failure probability based on point evolution kernel density and adaptive subset simulation that effectively improves computational efficiency.

Time-variant reliability problems, which often invoke multiple failure modes, have witnessed significant advancements due to the development of the outcrossing rate and its enhanced variants. However, in practical engineering applications, structures/systems are generally susceptible to complex system reliability issues. The complexity stems from time-variant parameters of stiffness, strength, vibration frequency, and various failure modes. Despite the outperformance of outcrossing methods in reliability analysis, their practical application in system-level reliability assessment remains elusive [1]. Hagen and Tvedt [29] introduced a time-variant system reliability method based on the crossover rate, focusing on boundary reduction in system response through binary response combinations. Dey and Mahadevan [30] proposed an adaptive importance sampling method to estimate structural system reliability subject to dynamic loads and drag. Son and Savage [31] developed a design-phase analysis approach for assessing a multi-time-variant response system reliability, attending to the degradation of structural components. Burgazzi [32] introduced a method to address the challenges imposed by systems that undergo non-stationary stochastic processes during operation. Gupta *et al* [33] proposed a time-variant reliability analysis method, which was applied to assess the reliability of series systems with lognormal vector responses. Despite progress in the study of time-variant system reliability, a number of technical challenges remain to hinder practical engineering applications. Existing methods are still limited to specific cases, such as series or parallel systems. Versatile models that can be applied in series, parallel, and hybrid systems [1] are yet to be formulated. To this gap, Jiang *et al* [20] developed the TRPD method, which is applicable to all the aforementioned systems. The stochastic process discretization of TRPDs is similar to Monte Carlo simulation (MCS) in that accuracy increases with the number of discrete moments. Nevertheless, as the number of discrete stochastic processes and time intervals increase, the computational time increases exponentially. To enhance computational efficiency, the number of discretized stochastic processes should be low, which is again susceptible to instability in reliability results. Thus, it is imperative to develop a computationally efficient method that is versatile for generic structural system problems.

To this end, this study proposes a new method that integrates the Kriging model with stochastic process discretization. The currently proposed approach achieves higher computational efficiency and entails fewer function calls. It is viable for handling a broad range of structural systems. A note of attention is that the currently proposed method, by employing the Kriging model, can predict the most probable point (MPP) at more discrete time instants, thereby improving accuracy to some extent.

The remainder of this paper is organized as follows. Section 2 presents a reliability assessment of time-variant structural systems. Section 3 outlines the current K-TRPD algorithm. Section 4 presents a set of numerical and engineering examples to validate the currently proposed method. Section 5 concludes this study.

2. Preliminaries

2.1. Time-variant reliability problem with a single failure mode

Time-variant reliability of structures refers to the probability that a structure will fulfill its intended function within a specified time frame in spite of the influence of time-variant uncertainties. In this regard, the reliability over a given time interval can be expressed as

$$P_{\mathrm{s}}\left(0,\ t_{\mathrm{e}}\right)=P\left\{g\left(\mathbf{X},\mathbf{Y}\left(t\right),t\right)>0,\forall t\in\left[0,\ t_{\mathrm{e}}\right]\right\}, \tag{1}$$

where $g\left(\cdot\right)$ is the performance function of the structure; $\mathbf{X}=\left[X_1,X_2,\ldots,X_n\right]^{\mathrm{T}}$ denotes the random variable and $\mathbf{Y}\left(t\right)=\left[Y_1\left(t\right),Y_2\left(t\right),\ldots,Y_m\left(t\right)\right]$ represents the stochastic process.

For a structure, the failure probability over a time interval $\left[0,t_{\mathrm{e}}\right]$ can be formulated as

$$P_{\mathrm{f}}\left(0,t_{\mathrm{e}}\right)=\mathrm{Prob}\left(g\left(\mathbf{X},\mathbf{Y}\left(t\right),t\right)\leqslant 0,\exists t\in\left[0,t_{\mathrm{e}}\right]\right). \tag{2}$$

The mathematical expression for the outcrossing rate method is [34]

$$v^{+}\left(\tau\right)=\lim_{\Delta\tau\to 0,\Delta\tau>0}\frac{P\left[N^{+}\left(\tau,\tau+\Delta\tau\right)=1\right]}{\Delta\tau}, \tag{3}$$

where $N^{+}\left(\tau,\tau+\Delta\tau\right)$ is the number of times a structural performance function crosses from a safe region to a failure region

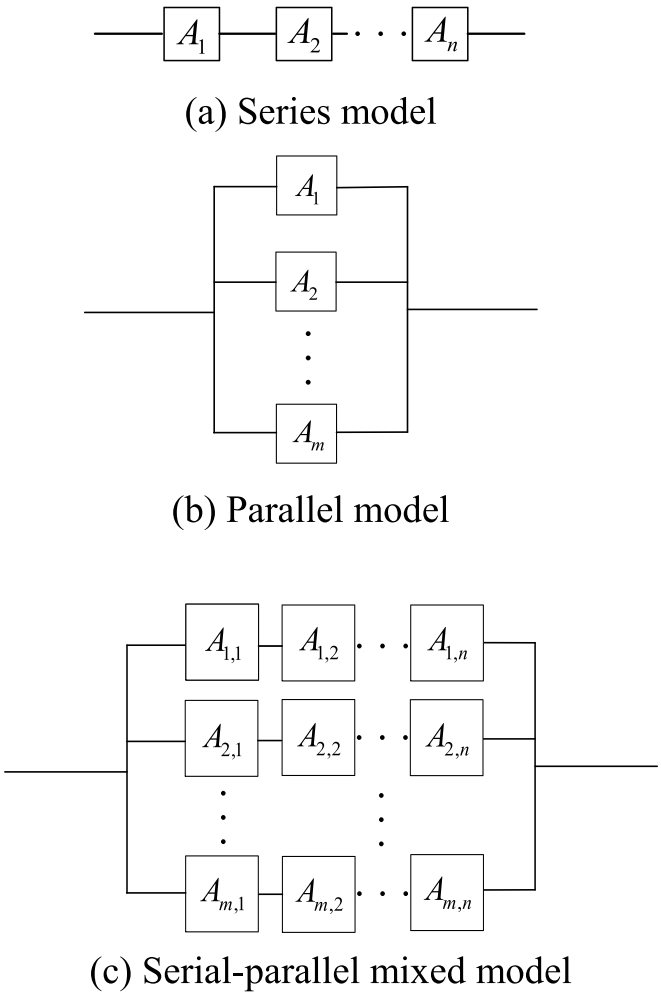

Figure 1. Schematic for different structural system models [1].

within the time interval $[\tau, \tau+\Delta\tau]$; $P[\cdot]$ refers to the probability of crossing the boundary once. The crossing rate can be expressed as [35]

$$v^{+}(\tau) = \lim_{\Delta\tau\to 0,\Delta\tau>0} \frac{P\{g(\mathbf{X},\mathbf{Y}(\tau),\tau)>0 \cap g(\mathbf{X},\mathbf{Y}(\tau+\Delta\tau),\tau+\Delta\tau)\leqslant 0\}}{\Delta\tau}. \quad (4)$$

It is assumed that the probability for the occurrence of a crossover rate event is marginal and it follows Poisson distribution with independent occurrences within the time interval $[\tau, \tau+\Delta\tau]$. Thus, equation (1) can be rewritten as [1]

$$P_s(0,t_e) = P_s(0)\exp\left[-\int_0^T v^{+}(t)\mathrm{d}t\right], \quad (5)$$

where $P_s(0)$ represents the structure's initial failure probability.

2.2. Reliability of the time-variant structural system

In terms of the correlative logic among different functional units, the structural system can be classified into series, parallel, and serial-parallel mixed models [1], as illustrated in figure 1.

To facilitate subsequent derivations, reliability events are introduced to represent the three system models. Reliability event E can be expressed as [1]

$$E = \left\{\bigcup_{i=1}^{a}\bigcap_{j=1}^{b} E_{i,j}\right\}, \quad (6)$$

where $E_{i,j}$ stands for the reliable events of functional units $B_{i,j}$; a and b represent order units in series and parallel models, respectively. If $a=1$, this event corresponds to a series system; if $b=1$, the event stands for a parallel system; otherwise, the event E represents a mixed system. In the structural system, the reliability of functional units $B_{i,j}$ refers to their instantaneous reliability at any given time instant throughout the entire lifecycle. Equation (1) can then be reformulated as

$$E = \left\{\bigcup_{i=1}^{a}\bigcap_{j=1}^{b}\{g_{i,j}(\mathbf{X},\mathbf{Y}(t),t)>0\}, \forall t\in[0,t_e]|\right\}, \quad (7)$$

where $g_{i,j}$ is performance function of the functional unit $B_{i,j}$. Reliability over a time interval $[0, t_e]$ is given by

$$P_s(0,t_e) = \mathrm{Prob}\left\{\bigcup_{i=1}^{a}\bigcap_{j=1}^{b}\{g_{i,j}(\mathbf{X}(t),\mathbf{Y},t)>0, \forall t\in[0,t_e]|\}\right\}. \quad (8)$$

MCS is usually employed to solve equation (8). This approach invokes numerous stochastic processes and variables to approximate the time-variant reliability. With a sufficient number of samples, this method achieves high accuracy. The add-value is that it is relatively straightforward to implement. However, it is computationally expensive, particularly for small failure probability problems that hinder the practical engineering application of MCS. The subsequent subsections will introduce a computational measure to tackle these issues.

2.3. Time-variant system reliability analysis method based on stochastic process discretization

In TRPDs, the stochastic process and time intervals are discretized prior to discretizing the performance function. Subsequently, the discrete stochastic processes and variables are mapped onto the normal space, where the performance function is approximated at the MPP using the first-order Taylor expansion. This process effectively transforms the time-variant system reliability problem into a time-independent one. Finally, the reliability of the time-independent system is evaluated.

Time interval $[0, t_e]$ is divided into p equal segments of $\Delta t = t_e/p$. Performance function is then divided accordingly.

The structure's reliability throughout the entire design lifecycle requires that the reliability at every instant should be accurate. Hence, equation (8) can be rewritten as

$$P_{\mathrm{s}}(0,t_{\mathrm{e}}) = \mathrm{Prob}\left\{\bigcup_{i=1}^{a}\bigcap_{j=1}^{b}\bigcap_{k=1}^{c}\left\{g_{i,j,k}(\mathbf{X},\mathbf{Y}_k,t_k)>0,\forall t_k\in[0,t_{\mathrm{e}}]\right\}\right\}, \tag{9}$$

where $g_{i,j,k}(\mathbf{X},\mathbf{Y}_k,t_k)$ denotes performance function at the time instant t_k; $\mathbf{Y}_k=[Y_1(t_k),Y_2(t_k),\ldots,Y_d(t_k)]^{\mathrm{T}}$ represents the random variable matrix of $c\times d$ dimension from time discretization of the stochastic process. From equation (9), all functions after time discretization contain only random variables. For convenience of derivation, the Nataf transform [36] is introduced to convert random variables into standard normal variables. Thus, equation (9) can be rewritten as

$$P_{\mathrm{s}}(0,t_{\mathrm{e}}) = \mathrm{Prob}\left\{\bigcup_{i=1}^{a}\bigcap_{j=1}^{b}\bigcap_{k=1}^{c}\left\{G_{i,j,k}(\mathbf{V},\mathbf{U}_k,t_k)>0,\forall t_k\in[0,t_{\mathrm{e}}]\right\}\right\}, \tag{10}$$

where $\mathbf{V}$ and $\mathbf{U}$ are representations of $\mathbf{X}$ and $\mathbf{Y}(t)$ in standard normal space. The specific transformations can be expressed as

$$\left[\left(\mathbf{U}_1^{\mathrm{T}},\mathbf{U}_2^{\mathrm{T}},\ldots,\mathbf{U}_c^{\mathrm{T}}\right)^{\mathrm{T}};\boldsymbol{\rho}_{\mathbf{U}}\right] = \mathrm{Nataf}\left[\left(\mathbf{Y}_1^{\mathrm{T}},\mathbf{Y}_2^{\mathrm{T}},\ldots,\mathbf{Y}_c^{\mathrm{T}}\right)^{\mathrm{T}};\boldsymbol{\rho}_{\mathbf{Y}}\right], \tag{11}$$

$$(\mathbf{V};\boldsymbol{\rho}_{\mathbf{V}}) = \mathrm{Nataf}(\mathbf{X};\boldsymbol{\rho}_{\mathbf{X}}), \tag{12}$$

where $\boldsymbol{\rho}_{\mathbf{X}}$ and $\boldsymbol{\rho}_{\mathbf{Y}}$ denote correlation coefficient matrixes. For each discrete function, the FORM is used to calculate its MPP, followed by a first-order Taylor expansion at the MPP. The corresponding transformations can be formulated as

$$P_{\mathrm{s}}(0,t_{\mathrm{e}}) = \mathrm{Prob}\left\{\bigcup_{i=1}^{a}\bigcap_{j=1}^{b}\bigcap_{k=1}^{c}\left[\sum_{l=1}^{d}\left.\frac{\partial G_{i,j,k}}{\partial U'_{k,l}}\right|_{U''_{i,j,k,l}}\left(U'_{k,l}-U''_{i,j,k,l}\right)+\sum_{m=1}^{f}\left.\frac{\partial G_{i,j,k}}{\partial V'_{m}}\right|_{V''_{i,j,k,m}}\left(V'_{m}-V''_{i,j,k,m}\right)>0\right]\right\}, \tag{13}$$

where $(U''_{i,j,k},V''_{i,j,k})$ denotes the MPP of $G_{i,j,k}(\mathbf{V},\mathbf{U}_k,t_k)$; $(\mathbf{U}'_k,\mathbf{V}')$ represents the mean of a random variable of kth performance function and a stochastic process; $U'_{k,l}$ stands for the lth discrete random variable; and V'_m refers to the mth discrete random variable. $Q_{i,j}$ is then imported to solve equation (13). It is assumed that the cumulative distribution function is $F_{Q_{i,j}}$, and $Q_{i,j}$ does not affect the final result of equation (13) [1]. For convenience of analysis, it is assumed in the following derivation that $Q_{i,j}$ follows a standard normal distribution. Thus, equation (13) becomes

$$P_{\mathrm{s}}(T) = \mathrm{Prob}\left\{\bigcup_{i=1}^{a}\bigcap_{j=1}^{b}\left\{F_{Q_{i,j}}^{-1}\left\{\Phi_c\left\{\left[\sum_{l=1}^{d}\left.\frac{\partial G_{i,j,k}}{\partial U'_{k,l}}\right|_{U_{i,j,k,l}}\left(-U''_{i,j,k,l}\right)+\sum_{m=1}^{f}\left.\frac{\partial G_{i,j,k}}{\partial V'_{m}}\right|_{V'_{i,j,k,m}}\left(V'_{m}-V''_{i,j,k,m}\right)\right],\boldsymbol{\mu}_{\boldsymbol{\theta}_{i,j}},\mathbf{C}_{\boldsymbol{\theta}_{i,j}}\right\}\right\}-Q_{i,j}>0\right\}\right\}, \tag{14}$$

where $F_{Q_{i,j}}(\cdot)$ denotes the distribution function of $Q_{i,j}$; $F_{Q_{i,j}}^{-1}(\cdot)$ is the inverse function of $F_{Q_{i,j}}$; $\boldsymbol{\mu}_{\boldsymbol{\theta}_{i,j}}$ and $\mathbf{C}_{\boldsymbol{\theta}_{i,j}}$ refer to the mean and covariance matrix of $\boldsymbol{\theta}_{i,j}=\left[(\theta_{i,j})_1,(\theta_{i,j})_2,\ldots,(\theta_{i,j})_c\right]^{\mathrm{T}}$. $(\theta_{i,j})_k$ can be expressed as

$$(\theta_{i,j})_k = -\sum_{j=1}^{m}\frac{\partial G_{i,j,k}}{\partial U'_{k,j}}\Big|_{U'_{i,j,k,l}}U'_{k,j},\ k=1,2,\ldots,c. \tag{15}$$

Although equation (15) is more effective than equation(13), it uses the FORM to estimate the MPPs of all discrete values. As the discrete values increase, the computational cost also increases substantially. Thus, when TRPDs are applied to time-variant system reliability analysis, computational efficiency decreases as the number of discretizations increases.

3. Currently proposed method

The K-TRPD method incorporates the Kriging model to calculate the MPP for each discrete function. The K-TRPD method in this study calculates the MPP at some time instants exclusively, and uses fewer time points than the TRPD method. This substantially reduces the invocation of the FORM. The Kriging model is then constructed using the calculated MPP to approximate the MPP of the time interval. This approach circumvents continuous reliability analysis of each failure mode, thereby reducing the number of function calls required to solve time-variant system reliability analysis.

3.1. System time-variant reliability analysis method

In standard normal space, the MPP of the performance function at t_k, $(k=1,2,\ldots,q)$ is $\mathbf{Z}_{\mathrm{MPP}(t_k)}^{(i,j)}=\left[\mathbf{U}_{\mathrm{MPP}}^{(i,j,k)},\mathbf{V}_{\mathrm{MPP}}^{(i,j,k)}\right]$, which can be calculated by the following equation,

$$\begin{cases}\text{find} & \mathbf{Z}_{\mathrm{MPP}}=\min\beta_{\mathrm{r}}\\ \text{s.t.} & G(\mathbf{Z}_{\mathrm{MPP}})=0\end{cases}, \tag{16}$$

where β_{r} denotes the reliability index and $\left(t_j,\mathbf{Z}_{\mathrm{MPP}(t_k)}^{(i,j)}\right)$ are used as training samples of Kriging model. The discrete time points t_j are taken as the input of the Kriging model, and the initial model is constructed to predict the MPP at each discrete

time instant. Equation (13) can then be rewritten as

$$P_{\mathrm{s}}(0,t_{\mathrm{e}}) = \mathrm{Prob}\left\{ \bigcup_{i=1}^{a} \bigcap_{j=1}^{b} \bigcap_{k=1}^{c} \left[\left. \frac{\partial G_{i,j,k}}{\partial \mathbf{U}_k} \right|_{\mathfrak{C}_{\mathrm{MPP}}^{(i,j,k)}} \left(\mathbf{U}_k - \hat{\mathbf{U}}_{\mathrm{MPP}}^{(i,j,k)} \right) + \left. \frac{\partial G_{i,j,k}}{\partial \mathbf{V}} \right|_{\hat{\mathbf{V}}_{\mathrm{MPP}}^{(i,j,k)}} \left(\mathbf{V} - \hat{\mathbf{V}}_{\mathrm{MPP}}^{(i,j,k)} \right) > 0 \right] \right\}, \tag{17}$$

where $\left(\hat{\mathbf{U}}_{\mathrm{MPP}}^{(i,j,k)}, \hat{\mathbf{V}}_{\mathrm{MPP}}^{(i,j,k)}\right)$ denotes the MPP at discrete time instant $t_k\,(k=1,2,\ldots,c)$.

3.1.1. Series system. In a series system, the failure of any individual subsystem leads to failure of the overall system. Accordingly, for a series system, equation (17) can be expressed as follows,

$$P_{\mathrm{s}}(0,t_{\mathrm{e}}) = \mathrm{Prob}\left\{ \bigcap_{j=1}^{b} \bigcap_{k=1}^{c} \left[\left. \frac{\partial G_{j,k}}{\partial \mathbf{U}_k} \right|_{\mathfrak{C}_{\mathrm{MPP}}^{(j,k)}} \left(\mathbf{U}_k - \hat{\mathbf{U}}_{\mathrm{MPP}}^{(j,k)} \right) + \left. \frac{\partial G_{j,k}}{\partial \mathbf{V}} \right|_{\hat{\mathbf{V}}_{\mathrm{MPP}}^{(j,k)}} \left(\mathbf{V} - \hat{\mathbf{V}}_{\mathrm{MPP}}^{(j,k)} \right) > 0 \right] \right\}. \tag{18}$$

Equation (18) can be further rewritten as

$$P_{\mathrm{s}}(0,t_{\mathrm{e}}) = \mathrm{Prob}\left\{ \bigcap_{j=1}^{b} \bigcap_{k=1}^{c} \left[\left. \frac{\partial G_{j,k}}{\partial \mathbf{U}_k} \right|_{\mathfrak{C}_{\mathrm{MPP}}^{(j,k)}} \left(-\hat{\mathbf{U}}_{\mathrm{MPP}}^{(j,k)} \right) + \left. \frac{\partial G_{j,k}}{\partial \mathbf{V}} \right|_{\hat{\mathbf{V}}_{\mathrm{MPP}}^{(j,k)}} \left(\mathbf{V} - \hat{\mathbf{V}}_{\mathrm{MPP}}^{(j,k)} \right) > \left. \frac{\partial G_{j,k}}{\partial \mathbf{U}_k} \right|_{\hat{\mathbf{U}}_{\mathrm{MPP}}^{(j,k)}} \mathbf{U}_k \right] \right\}. \tag{19}$$

To solve equation (19), a random variable $\boldsymbol{\alpha}_j = [\alpha_{j,1}, \alpha_{j,k}, \ldots, \alpha_{j,k}]^{\mathrm{T}}$ is introduced, in which the mean value is $\boldsymbol{\mu}_{\boldsymbol{\alpha}_j}$ and the correlation coefficient matrix is $\mathbf{C}_{\boldsymbol{\alpha}_j}$:

$$\alpha_{j,k} = \left. \frac{\partial G_{j,k}}{\partial \mathbf{U}_k} \right|_{\hat{\mathbf{U}}_{\mathrm{MPP}}^{(j,k)}} \mathbf{U}_k. \tag{20}$$

Introducing the random variable Q_j into equation (20) yields

$$\breve{g}_j(\mathbf{V}, Q_j) = F_{Q_j}^{-1}\left\{ \Phi_c\left\{ \left[G'_{\mathbf{U}_{j,k}}\left(-\mathbf{U}_{\mathrm{MPP}}^{(j,k)}\right) + G'_{\mathbf{V}_{j,k}}\left(\mathbf{V} - \mathbf{V}_{\mathrm{MPP}}^{(j,k)}\right) \right], \boldsymbol{\mu}_{\boldsymbol{\alpha}_j}, \mathbf{C}_{\boldsymbol{\alpha}_j} \right\} \right\} - Q_j, \tag{21}$$

where $G'_{\mathbf{U}_{j,k}}$ and $G'_{\mathbf{V}_{j,k}}$ are the partial derivatives of the performance function at the MPP:

$$G'_{\mathbf{U}_{j,k}} = \left. \frac{\partial G_{j,k}}{\partial \mathbf{U}_k} \right|_{\mathfrak{C}_{\mathrm{MPP}}^{(j,k)}} \tag{22}$$

$$G'_{\mathbf{V}_{j,k}} = \left. \frac{\partial G_{j,k}}{\partial \mathbf{V}} \right|_{\mathbf{V}_{\mathrm{MPP}}^{(j,k)}}. \tag{23}$$

Equation (23) can then be rewritten as

$$P_{\mathrm{s}}(0,t_{\mathrm{e}}) = \mathrm{Prob}\left\{ \bigcap_{j=1}^{b} \left[\breve{g}_j(\mathbf{V}, Q_j) > 0 \right] \right\}, \tag{24}$$

where the random variables $\mathbf{V}$ and Q_j are independent of the time variable t. Equation (21) can be further rewritten as

$$\breve{g}_j(\mathbf{Z}_j) = F_{Q_j}^{-1}\left\{ \Phi_c\left\{ \left[G'_{\mathbf{U}_{j,k}}\left(-\mathbf{U}_{\mathrm{MPP}}^{(j,k)}\right) + G'_{\mathbf{V}_{j,k}}\left(\mathbf{V} - \mathbf{V}_{\mathrm{MPP}}^{(j,k)}\right) \right], \boldsymbol{\mu}_{\boldsymbol{\alpha}_j}, \mathbf{C}_{\boldsymbol{\alpha}_j} \right\} \right\} - Q_j, \tag{25}$$

where $\mathbf{Z}_j = [\mathbf{V}, Q_j]$ represents the random variable of the performance function. $\breve{g}_j(\mathbf{Z}_j)$ can be converted into the standard normal space by

$$\breve{G}_j(\mathbf{Z'}_j) = \mathrm{T}_j(\mathbf{V'}) - Q_j \tag{26}$$

where $\mathbf{V'}$ is the transformation of $\mathbf{V}$ in the standard normal space. When equation (26) is expanded into a Taylor series at the MPP. Retaining only the first term, the expansion can be written as

$$\breve{G}_j(\mathbf{Z'}_j)_L = \left\| \nabla \breve{G}_j\left(\mathbf{Z'}_j^*\right) \right\| \left(\beta_j - \alpha_j^{\mathrm{T}} \mathbf{Z'}_j\right). \tag{27}$$

Substituting equation (27) into equations (24) and (26) can then be further rewritten as

$$P_{\mathrm{s}}(0,t_{\mathrm{e}}) = \mathrm{Prob}\left\{ \bigcap_{j=1}^{b} \left[\left\| \nabla \breve{G}_j\left(\mathbf{Z'}_j^*\right) \right\| \left(\beta_j - \alpha_j^{\mathrm{T}} \mathbf{Z'}_j\right) > 0 \right] \right\}, \tag{28}$$

where $\mathbf{Z'}_j^*$ is the MPP of performance function $\breve{G}_j(\mathbf{Z'}_j)$; β_j and $\mathbf{Z'}_j^*$ can be determined through following optimization,

$$\begin{cases} \text{find } \mathbf{Z'}_j = \min \beta_j \\ \text{s.t. } \breve{G}_j(\mathbf{Z'}_j) = 0 \end{cases}. \tag{29}$$

Equation (29) can then be further rewritten as

$$P_{\mathrm{s}}(0,t_{\mathrm{e}}) = \mathrm{Prob}\left\{ \bigcup_{j=1}^{a} \left[\beta_j > \alpha_j^{\mathrm{T}} \mathbf{Z'}_j \right] \right\}, \tag{30}$$

where $\boldsymbol{\alpha}_j$ is the unit vector of the performance function at the MPP, which can be rewritten as

$$\boldsymbol{\alpha}_j = -\frac{\nabla \breve{G}_j\left(\mathbf{Z'}_j^*\right)}{\left\| \nabla \breve{G}_j\left(\mathbf{Z'}_j^*\right) \right\|}, j = 1,2,\ldots,b. \tag{31}$$

According to $\breve{G}_j\left(\mathbf{Z'}_j\right)_L (j=1,2,\ldots,b)$, the correlation coefficient between different failure mode functions can be calculated by

$$\rho_{j,j+1}=\frac{\mathrm{Cov}\left(\breve{G}_j\left(\mathbf{Z'}_j\right)_L,\breve{G}_{j+1}\left(\mathbf{Z'}_{j+1}\right)_L\right)}{\sigma_{\breve{G}_j\left(\mathbf{Z'}_j\right)_L}\sigma_{\breve{G}_{j+1}\left(\mathbf{Z'}_{j+1}\right)_L}}, \tag{32}$$

where $\mathrm{Cov}(\breve{G}_j\left(\mathbf{Z'}_j\right)_L,\breve{G}_{j+1}\left(\mathbf{Z'}_{j+1}\right)_L)$ is the covariance matrix between different failure modes. The reliability of the series system can be derived by solving equation (32).

3.1.2. Parallel system. In a parallel system, as long as a single part of the structure does not fail, the system will not fail. Thus, for a parallel system, equation (17) can be rewritten as

$$P_{\mathrm{s}}(0,t_{\mathrm{e}})=\mathrm{Prob}\left\{\bigcup_{i=1}^{a}\bigcap_{k=1}^{c}\left[\frac{\partial G_{i,k}}{\partial \mathbf{U}_k}\Big|_{\mathfrak{u}_{\mathrm{MPP}}^{(i,k)}}\left(\mathbf{U}_k-\hat{\mathbf{U}}_{\mathrm{MPP}}^{(i,k)}\right)+\frac{\partial G_{i,k}}{\partial \mathbf{V}}\Big|_{\hat{\mathbf{V}}_{\mathrm{MPP}}^{(i,k)}}\left(\mathbf{V}-\hat{\mathbf{V}}_{\mathrm{MPP}}^{(i,k)}\right)>0\right]\right\}. \tag{33}$$

Equation (33) can be further rewritten as

$$P_{\mathrm{s}}(0,t_{\mathrm{e}})=\mathrm{Prob}\left\{\bigcup_{i=1}^{a}\bigcap_{k=1}^{c}\left[\frac{\partial G_{i,k}}{\partial \mathbf{U}_k}\Big|_{\mathfrak{u}_{\mathrm{MPP}}^{(i,k)}}\left(-\hat{\mathbf{U}}_{\mathrm{MPP}}^{(i,k)}\right)+\frac{\partial G_{i,k}}{\partial \mathbf{V}}\Big|_{\hat{\mathbf{V}}_{\mathrm{MPP}}^{(i,k)}}\left(\mathbf{V}-\hat{\mathbf{V}}_{\mathrm{MPP}}^{(i,k)}\right)>\frac{\partial G_{i,k}}{\partial \mathbf{U}_k}\Big|_{\mathfrak{U}_{\mathrm{MPP}}^{(i,k)}}\mathbf{U}_k\right]\right\}. \tag{34}$$

To solve equation (34), a random variable $\boldsymbol{\alpha}_i=[\alpha_{i,1},\alpha_{i,k},\ldots,\alpha_{i,k}]^{\mathrm{T}}$ is introduced to take the form of

$$\alpha_{i,k}=\frac{\partial G_{i,k}}{\partial \mathbf{U}_k}\Big|_{\hat{\mathfrak{U}}_{\mathrm{MPP}}^{(i,k)}}\mathbf{U}_k. \tag{35}$$

Introducing the random variable Q_j into equation (34) yields

$$\breve{g}_i(\mathbf{V},Q_i)=F_{Q_i}^{-1}\left\{\Phi_c\left\{\left[G'_{\mathbf{U}_{i,k}}\left(-\mathbf{U}_{\mathrm{MPP}}^{(i,k)}\right)+G'_{\mathbf{V}_{i,k}}\left(\mathbf{V}-\mathbf{V}_{\mathrm{MPP}}^{(i,k)}\right)\right],\boldsymbol{\mu}_{\boldsymbol{\alpha}_i},\mathbf{C}_{\boldsymbol{\alpha}_i}\right\}\right\}-Q_i>0, \tag{36}$$

where $G'_{\mathbf{V}_{i,k}}$ and $G'_{\mathbf{V}_{i,k}}$ denote partial derivatives of performance functions at the MPP:

$$G'_{\mathbf{U}_{i,k}}=\frac{\partial G_{i,k}}{\partial \mathbf{U}_k}\Big|_{\mathbf{U}_{\mathrm{MPP}}^{(i,k)}} \tag{37}$$

$$G'_{\mathbf{V}_{i,k}}=\frac{\partial G_{i,k}}{\partial \mathbf{V}}\Big|_{\mathbf{V}_{\mathrm{MPP}}^{(i,k)}}. \tag{38}$$

Equation (33) can be rewritten as

$$P_{\mathrm{s}}(0,t_{\mathrm{e}})=\mathrm{Prob}\left\{\bigcup_{i=1}^{a}\left[\breve{g}_i(\mathbf{V},Q_i)>0\right]\right\}, \tag{39}$$

where $\mathbf{V}$ and Q_i are independent of the time variable t. Equation (36) can then be further rewritten as

$$\breve{g}_i(\mathbf{Z}_i)=F_{Q_i}^{-1}\left\{\Phi_c\left\{\left[G'_{\mathbf{U}_{i,k}}\left(-\mathbf{U}_{\mathrm{MPP}}^{(i,k)}\right)+G'_{\mathbf{V}_{i,k}}\left(\mathbf{V}-\mathbf{V}_{\mathrm{MPP}}^{(i,k)}\right)\right],\boldsymbol{\mu}_{\boldsymbol{\alpha}_i},\mathbf{C}_{\boldsymbol{\alpha}_i}\right\}\right\}-Q_i, \tag{40}$$

where $\mathbf{Z}_i=[\mathbf{V},Q_i]$ is the random variable of the performance function $\breve{g}_i(\cdot)$, which will be transformed into the standard normal space. Equation (40) can then be rewritten as

$$\breve{G}_i\left(\mathbf{Z'}_i\right)=\mathrm{T}_i\left(\mathbf{V'}\right)-Q_i, \tag{41}$$

where $\mathbf{V'}$ is transformation of $\mathbf{V}$ in the standard normal space. When Taylor series expansion is performed on equation (41) at the MPP, the expansion can be expressed as

$$\breve{G}_i(\mathbf{Z'}_i)_L=\left\|\nabla\breve{G}_i\left(\mathbf{Z'}_i^*\right)\right\|\left(\beta_i-\alpha_i^{\mathrm{T}}\mathbf{Z'}_i\right). \tag{42}$$

Substituting equation (42) into equation (39), and equation(39) becomes

$$P_{\mathrm{s}}(0,t_{\mathrm{e}})=\mathrm{Prob}\left\{\bigcup_{i=1}^{a}\left[\left\|\nabla\breve{G}_i\left(\mathbf{Z'}_i^*\right)\right\|\left(\beta_i-\alpha_i^{\mathrm{T}}\mathbf{Z'}_i\right)>0\right]\right\}, \tag{43}$$

where $\mathbf{Z'}_i^*$ is the MPP of performance function $\breve{G}_i\left(\mathbf{Z'}_i\right)$; β_i and $\mathbf{Z'}_i^*$ can be determined through following optimization problem,

$$\begin{cases}\text{find } \mathbf{Z'}_i=\min\beta\\ \text{s.t. } \breve{G}_i\left(\mathbf{Z'}_i\right)=0\end{cases}. \tag{44}$$

Equation (43) can be then rewritten as

$$P_{\mathrm{s}}(0,t_{\mathrm{e}})=\mathrm{Prob}\left\{\bigcup_{i=1}^{a}\left[\beta_i>\alpha_i^{\mathrm{T}}\mathbf{Z'}_i\right]\right\}, \tag{45}$$

where $\boldsymbol{\alpha}_i$ stands for the unit vector of the performance function at $\mathbf{Z'}_i^*$

$$\boldsymbol{\alpha}_i=-\frac{\nabla\breve{G}_i\left(\mathbf{Z'}_i^*\right)}{\left\|\nabla\breve{G}_i\left(\mathbf{Z'}_i^*\right)\right\|},i=1,2,\ldots,a. \tag{46}$$

According to $\breve{G}_i(\mathbf{Z'}_i)_L(i=1,2,\ldots,a)$, the correlation coefficient between different failure mode functions can be

calculated by

$$\rho_{i,i+1}=\frac{\mathrm{Cov}\left(\breve{G}_i(\mathbf{Z'}_i)_L,\breve{G}_{i+1}(\mathbf{Z'}_{i+1})_L\right)}{\sigma_{\breve{G}_i(\mathbf{Z'}_i)_L}\sigma_{\breve{G}_{i+1}(\mathbf{Z'}_{i+1})_L}},\tag{47}$$

where $\mathrm{Cov}(\breve{G}_i(\mathbf{Z'}_i)_L,\breve{G}_{i+1}(\mathbf{Z'}_{i+1})_L)$ is the covariance matrix between different failure modes. The reliability of the parallel system can be acquired by solving equation (45).

3.2. Construction of Kriging models for each failure mode

3.2.1. Fundamentals of the Kriging model. The time-variant reliability analysis method using surrogate model generally incorporates approaches such as a response surface [37], neural network [38], and the Kriging model [39]. These surrogate models can replace complex performance functions to improve computational efficiency. Among these models, the Kriging model stands out as a semi-parametric method that, unlike fully parameterized models, does not depend on a predefined mathematical formula, thus exhibiting great flexibility in application. The add-value of the Kriging model is that is minimizes prediction errors [40, 41]. Expositions of the Kriging model can be found in [42] and [39].

The Kriging model is composed of two components: a linear regression and stochastic process [43]. The general expression of the Kriging model is [44]

$$g(\mathbf{x})=\mathbf{f}^{\mathrm{T}}(\mathbf{x})\boldsymbol{\beta}+z(\mathbf{x}),\tag{48}$$

where $\mathbf{f}(\mathbf{x})=[f_1(\mathbf{x}),f_2(\mathbf{x}),\ldots,f_n(\mathbf{x})]^{\mathrm{T}}$ denotes the basic function; $\boldsymbol{\beta}=[\beta_1,\beta_2,\ldots,\beta_n]^{\mathrm{T}}$ represents the vector of the regression coefficient; $z(\mathbf{x})$ specifies the stationary Gaussian process, and its covariance function is [44]

$$\mathrm{cov}(z(\mathbf{x}_i),z(\mathbf{x}_j))=\sigma^2R(\mathbf{x}_i,\mathbf{x}_j),\ (i,j=1,2,\ldots,m),\tag{49}$$

where $R(\mathbf{x}_i,\mathbf{x}_j)$ is correlation coefficient of sample $\mathbf{x}_i$ and $\mathbf{x}_j$; m represents the number of $\mathbf{x}_i$; and σ^2 symbolizes the variance. $R(\mathbf{x}_i,\mathbf{x}_j)$ is expressed as [44]

$$R(\mathbf{x}_i,\mathbf{x}_j)=\exp\left(-\sum_{l=1}^{K}\theta_l(x_{i,l}-x_{j,l})^2\right),\tag{50}$$

where K refers to the dimension of variables and θ_l indicates the lth parameter.

The parameters in equation (48) can be computed individually [44]

$$\hat{\boldsymbol{\beta}}=\left(\mathbf{F}^{\mathrm{T}}\mathbf{R}^{-1}\mathbf{F}\right)^{-1}\mathbf{F}^{-1}\mathbf{R}^{-1}\mathbf{Y}\tag{51}$$

$$\hat{\sigma}^2=\frac{1}{m}\left(\mathbf{Y}-\boldsymbol{F}\hat{\boldsymbol{\beta}}\right)^{\mathrm{T}}\mathbf{R}^{-1}\left(\mathbf{Y}-\boldsymbol{F}\hat{\boldsymbol{\beta}}\right),\tag{52}$$

where $\mathbf{F}$ specifies the representation matrix $F_{ih}=f_h(\mathbf{x}_i)$. Each matrix element $\mathbf{R}$ is constituted of $R_{i,j}=R(\mathbf{x}_i,\mathbf{x}_j)$ [44]:

$$\mathbf{R}=\begin{bmatrix}R(\mathbf{x}_1,\mathbf{x}_1) & \cdots & R(\mathbf{x}_1,\mathbf{x}_j)\\ \vdots & \ddots & \vdots\\ R(\mathbf{x}_i,\mathbf{x}_1) & \cdots & R(\mathbf{x}_i,\mathbf{x}_j)\end{bmatrix}.\tag{53}$$

To estimate the relevant parameters, the maximum-likelihood estimation function can be derived as follows [44],

$$L=-\frac{1}{2}\left(n\ln\left(\hat{\sigma}^2\right)-\frac{1}{2}\ln|\mathbf{R}|\right).\tag{54}$$

The Kriging model response's optimal linear unbiased prediction and the mean squared error can be formulated as follows [44],

$$\hat{g}(\mathbf{x})=\mathbf{f}^{\mathrm{T}}(\mathbf{x})\hat{\boldsymbol{\beta}}+\mathbf{r}^{\mathrm{T}}(\mathbf{x})\mathbf{R}^{-1}\left(\mathbf{Y}-\boldsymbol{F}\hat{\boldsymbol{\beta}}\right)\tag{55}$$

$$\hat{\sigma}^2_{\hat{g}(\mathbf{X})}=\sigma^2\left(1+\mathbf{u}^{\mathrm{T}}\left(\mathbf{F}^{\mathrm{T}}\mathbf{R}^{-1}\mathbf{F}\right)^{-1}\mathbf{u}-\mathbf{r}^{\mathrm{T}}(\mathbf{x})\mathbf{R}^{-1}\mathbf{r}\right),\tag{56}$$

where $\mathbf{r}^{\mathrm{T}}(\mathbf{x})$ is the vector for the correlation of $\mathbf{x}$ and $\mathbf{u}=\mathbf{F}^{\mathrm{T}}\mathbf{R}^{-1}\mathbf{r}(\mathbf{x})-\mathbf{f}(\mathbf{x})$.

3.2.2. Prediction of MPP trajectory for each failure mode. To improve both the convergence performance and accuracy of the model, this study incorporates an active learning approach. It enhances the prediction of the trajectory for the maximum possible failure point in each failure mode. By leveraging active learning, more efficient sample points are selected, leading to a more accurate Kriging model. The most commonly used active learning functions are U [45], EFF [46] and ERF [47].

In TRPDs, the time interval $[0,\ t_e]$ is discretized into p equal time intervals $[t_i,\ t_{i+1}]$, $(i=1,2,\ldots,p)$, and the performance function $g(\mathbf{X},\mathbf{Y}(t),t)$ is discretized as $g_i(\mathbf{X},\mathbf{Y}(t_i),t_i)$ at each discrete time point t_i accordingly. We can select $q\,(q<p)$ time points from the entire discrete time instants to conduct the required MPP search. We define the MPP of the performance function at time $t_j\,(j=1,2,\ldots,q)$ in the standard normal space as $\mathbf{Z}_{\mathrm{MPP}}(t_j)=\left[\mathbf{V}^{(j)}_{\mathrm{MPP}},\mathbf{U}^{(j)}_{\mathrm{MPP}}\right]$. The obtained MPPs are regarded as the training samples $(t_j,\mathbf{Z}_{\mathrm{MPP}}(t_j))\,(j=1,2,\ldots,q)$ of the Kriging model, which is a single input (i.e. t) but multiple outputs (i.e. $\mathbf{Z}_{\mathrm{MPP}}=[\mathbf{V}_{\mathrm{MPP}},\mathbf{U}_{\mathrm{MPP}}]$). The mapping relationship between the inputs and the outputs can be expressed as

$$\begin{bmatrix}t_1\\ t_2\\ \vdots\\ t_q\end{bmatrix}\rightarrow\begin{bmatrix}\mathbf{Z}^{(1)}_{\mathrm{MPP}}\\ \mathbf{Z}^{(2)}_{\mathrm{MPP}}\\ \vdots\\ \mathbf{Z}^{(q)}_{\mathrm{MPP}}\end{bmatrix}.\tag{57}$$

Using these samples, a Kriging model $\hat{\mathbf{Z}}_{\mathrm{MPP}}(t)$ can be constructed based on the method depicted in Subsection 3.2.1. In

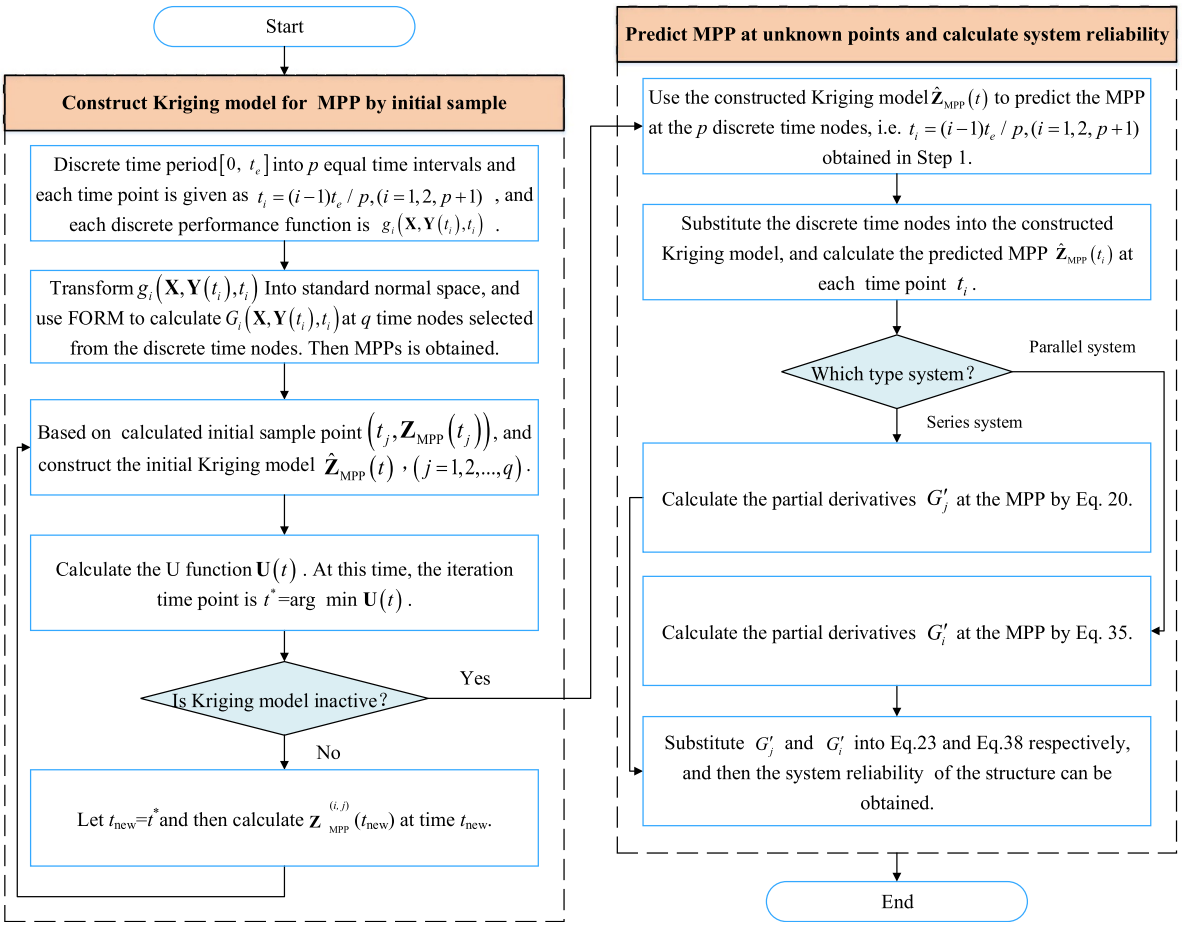

Figure 2. Flowchart for the proposed K-TRPD method.

building the Kriging model, the U function [45] is utilized to enhance the model's accuracy and efficiency:

$$U(\mathbf{X})=\frac{|\hat{g}(\mathbf{X})|}{\hat{\sigma}_{\hat{g}(\mathbf{X})}}, \tag{58}$$

where $\hat{g}(\mathbf{X})$ denotes the prediction of the Kriging model and $\hat{\sigma}_{\hat{g}(\mathbf{X})}$ is the corresponding standard deviation. Substituting the prediction of the Kriging model at discrete times into equation (58) leads to

$$\mathbf{U}(t_k)=\begin{cases}\dfrac{\left|\hat{\mathbf{Z}}_{\mathrm{MPP}}^{(i,j,k)}(t_k)\right|}{\hat{\boldsymbol{\sigma}}_{\hat{\mathbf{Z}}_{\mathrm{MPP}}^{(i,j,k)}}(t_k)} & i,j\neq 1 \text{ and } i,j>0\\ \dfrac{\left|\hat{\mathbf{Z}}_{\mathrm{MPP}}^{(j,k)}(t_k)\right|}{\hat{\boldsymbol{\sigma}}_{\hat{\mathbf{Z}}_{\mathrm{MPP}}^{(j,k)}}(t_k)} & i=1,j\neq 1\\ \dfrac{\left|\hat{\mathbf{Z}}_{\mathrm{MPP}}^{(i,k)}(t_k)\right|}{\hat{\boldsymbol{\sigma}}_{\hat{\mathbf{Z}}_{\mathrm{MPP}}^{(i,k)}}(t_k)} & i\neq 1,j=1\end{cases}, \tag{59}$$

where $\mathbf{U}(t_k)$ is the vector containing all components of the MPP; t_k is a random time instant within the time cycle and $\mathbf{U}(t)=(\mathbf{U}(t_1),\mathbf{U}(t_2),\ldots,\mathbf{U}(t_k))^{\mathrm{T}}$ denotes the matrix of $\mathbf{U}(t_k)$. The time instant at which the U function reaches its minimum value is identified during each iteration:

$$t^*=\underset{t\in[0,\ t_e]}{\arg\min}\,\mathbf{U}(t). \tag{60}$$

The FORM is then used to conduct time-invariant reliability analysis at the time instant t_{new} to derive MPP $\mathbf{Z}_{\mathrm{MPP}}^{(i,j)}(t_{\mathrm{new}})$, and the sample point $\left(t_{\mathrm{new}},\mathbf{Z}_{\mathrm{MPP}}^{(i,j)}(t_{\mathrm{new}})\right)$ is adopted as the initial sample.

The minimum value of $\mathbf{U}(t)$ is $\mathbf{U}(t_k)$ $(t_k\in[0,\ t_e])$; therefore, the termination criterion for updating of the U function in the Kriging model is

$$N=\begin{cases}N+1,t_{\mathrm{new}}=t^* & \min(\mathbf{U}(t_k))<2\\ N & \min(\mathbf{U}(t_k))\geqslant 2\end{cases}, \tag{61}$$

where N denotes the number of sample points. If $\min(\mathbf{U}(t_k))\leqslant 2$, the Kriging model should be updated. Otherwise, the Kriging model stops updating and predicting MPPs.

3.3. Procedure of the K-TRPD method

The K-TRPDs proposed in this study consists of below eight key steps. For illustrative purposes, a comprehensive flowchart is also presented in figure 2.

Step 1: The time interval and performance function are respectively discretized to p equal time intervals and $g_{i,j,k}(\mathbf{X},\mathbf{Y}(t_k),t_k)\ (k=1,2,\ldots,p)$.

Step 2: Nataf transformation is implemented to transform a random variable into a standard normal variable, and the performance function $g_{i,j,k}(\mathbf{X},\mathbf{Y}_k,t_k)$ is then transformed into $G_{i,j,k}(\mathbf{V},\mathbf{U}_k,t_k)$. Starting with $p+1$ discrete time points in Step 1, q time points are chosen at equal intervals. Subsequently, the FORM is applied to determine the MPP at each of these selected time points.

Step 3: According to q time points obtained in Step 2 and the corresponding MPPs, the initial sample point set is $(t_v,\mathbf{Z}_{\mathrm{MPP}}(t_v))\,(v=1,2,\ldots,q)$; the initial Kriging model can then be constructed.

Step 4: Introduce U function to update the Kriging model. According to the corresponding termination criteria, in each iteration, if one sample point is added and the new time instant is $t_{\mathrm{new}}=t^*$, time-invariant reliability analysis is conducted at the update time by utilizing the FORM to obtain the maximum possible failure point $\mathbf{Z}_{\mathrm{MPP}}^{(i,j)}(t_{\mathrm{new}})$. The sample point is then updated to the initial sample set and the Kriging model is updated. If $\min(\mathbf{U}(t_k))\geqslant 2$, the Kriging model stops updating.

Step 5: The Kriging model updated in Step 4 is used to predict the MPPs at p discrete time points. These MPPs are substituted into equation (27) for calculation.

Step 6: If the structural system is a series system, equation (18) is used to derive the solution. The partial derivative of the performance function $G_{j,k}(\mathbf{V},\mathbf{U}_k,t_k)$ at the MPP is $G'_j=\left(G'_{\mathbf{U}_{j,k}},G'_{\mathbf{V}_{j,k}}\right)$. If the structural system is a parallel system, equation (33) is used instead. The partial derivative of the performance function $G_{i,k}(\mathbf{V},\mathbf{U}_k,t_k)$ at the MPP is then calculated as $G'_i=\left(G'_{\mathbf{U}_{i,k}},G'_{\mathbf{V}_{i,k}}\right)$.

Step 7: Substituting $G'_i=\left(G'_{\mathbf{U}_{i,k}},G'_{\mathbf{V}_{i,k}}\right)$ in Step 6 into equations (21) and (36), respectively, the time-variant system reliability analysis can be transformed into time-invariant system reliability analysis.

Step 8: The FORM is used to solve equations (20) and (35), respectively, to derive the reliability of the structural system.

4. Exemplifications

4.1. Simply supported beam

Figure 3 illustrates the configuration of a simply supported beam. The length of the beam is 5 m. The overall simply supported beam sustains a cloth load $F(t)$. Considering the inevitable degradation of material properties with time, it is assumed that the flexural and shear strengths of simply supported beams follow the exponential decay model and the distributive stats are tabulated in table 1.

$$M(t)=M_0e^{-0.0005t} \tag{62}$$

$$V(t)=V_0e^{-0.0005t} \tag{63}$$

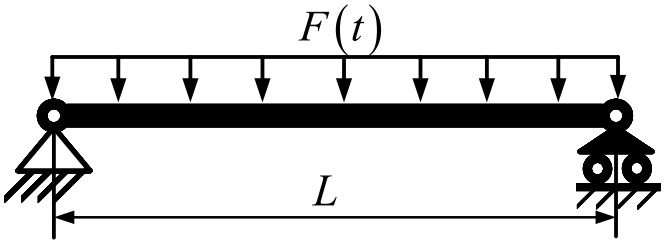

Figure 3. Simply supported beam [1, 20].

Table 1. Distributive stats of random variables for a simply supported beam.

Variables	Distribution	Mean	COV (%)	Acf.
M_0	Normal	800 kN	10	NA
V_0	Normal	700 kN	15	NA
$F(t)$	Gaussian process	120 kN m^{-1}	25	$\exp\left[-(2\tau)^2\right]$

In this example, five distinct circumstances (Cases 1–5) are examined. The time steps for each case are set to 1 year, 1/2 year, 2/5 year, 1/3 year, and 1/4 year, respectively. MCS, TRPDs and the currently proposed method are adopted to solve Cases 1–5. The resulting reliabilities are tabulated in table 2 and depicted in figure 4. A note of attention is that the samples are 10^6 for MCS. The results obtained by MCS are used as a metric to benchmark those by TRPDs and the currently proposed method.

From table 2, with decreasing time steps, the results from TRPDs and K-TRPDs approach those from MCS in Cases 1–5 with gradual improvement in accuracy. In Case 1, the highest error between the results by the two methods and MCS is 18.51%. However, with the increase in discrete numbers, the highest error between the results by the two methods is as low as 2.40% in Case 5. When a single failure mode is considered and at the time instant $t=10$, the reliability indexes are 2.3557 and 2.1497 in Case 5 by the two methods, respectively. The reliability index of the system considering the two series failure modes is 2.0162, which is lower than that of the single failure mode. In terms of calculation efficiency, with the decrease of time step Δt, the performance function calls of TRPDs increase more remarkably, from 200 of Case 1 to 800 of Case 5, while performance function calls of K-TRPDs increase gradually from 140 of Case 1 to 380 of Case 5. In Case 5, the performance function calls for K-TRPDs are only half that of TRPDs. Compared to the TRPD method, the currently proposed approach demonstrates improved computational efficiency.

4.2. Planar three-bar structure

Figure 5 shows a planar three-bar structure. The lengths of bars 1 and 3 are L, and the length of bar 2 is H. The load is applied at the junction and the material strength is η. For this structure, when the force is maximum, bar 2 fails first, and the structure is

Table 2. Reliability index for simply supported beams in 1–10 years.

Cases	Time/year	1	2	3	4	5	6	7	8	9	10	NoF
	MCS	2.6276	2.4604	2.3567	2.2748	2.2083	2.1586	2.1093	2.0678	2.0331	2.0022	10^6
Case 1 (%)	TRPDs	3.0225 (15.03)	2.8323 (15.11)	2.7189 (15.37)	2.6376 (15.95)	2.5740 (16.55)	2.5216 (16.82)	2.4771 (17.44)	2.4382 (17.92)	2.4038 (18.23)	2.3728 (18.51)	200
	K-TRPDs	3.0225 (15.03)	2.8323 (15.12)	2.7189 (15.37)	2.6376 (15.95)	2.5740 (16.56)	2.5216 (16.82)	2.4771 (17.44)	2.4382 (17.92)	2.4038 (18.23)	2.3728 (18.51)	**140**
Case 2 (%)	TRPDs	2.8440 (8.24)	2.6537 (7.86)	2.5391 (7.74)	2.4566 (7.99)	2.3920 (8.31)	2.3387 (8.34)	2.2934 (8.73)	2.2540 (9.00)	2.2189 (9.14)	2.1874 (9.25)	400
	K-TRPDs	2.8440 (8.24)	2.6537 (7.86)	2.5391 (7.74)	2.4566 (7.99)	2.3920 (8.31)	2.3387 (8.34)	2.2934 (8.73)	2.2540 (9.00)	2.2189 (9.14)	2.1874 (9.25)	**220**
Case 3 (%)	TRPDs	2.8517 (8.53)	2.6021 (5.76)	2.5065 (6.36)	2.4035 (5.66)	2.3503 (6.43)	2.2846 (5.84)	2.2475 (6.55)	2.1990 (6.34)	2.1703 (6.75)	2.1317 (6.46)	500
	K-TRPDs	2.8517 (8.53)	2.6021 (5.76)	2.5065 (6.36)	2.4035 (5.66)	2.3503 (6.43)	2.2846 (5.84)	2.2475 (6.55)	2.1990 (6.34)	2.1703 (6.75)	2.1317 (6.46)	**260**
Case 4 (%)	TRPDs	2.7525 (4.75)	2.5611 (4.09)	2.4449 (3.74)	2.3610 (3.79)	2.2952 (3.93)	2.2410 (3.82)	2.1948 (4.06)	2.1546 (4.20)	2.1187 (4.22)	2.0867 (4.22)	600
	K-TRPDs	2.7525 (4.75)	2.5611 (4.09)	2.4449 (3.74)	2.3610 (3.79)	2.2952 (3.93)	2.2410 (3.82)	2.1948 (4.06)	2.1546 (4.20)	2.1187 (4.22)	2.0866 (4.22)	**300**
Case 5 (%)	TRPDs	2.6906 (2.40)	2.4976 (1.51)	2.3798 (0.10)	2.2947 (0.09)	2.2280 (0.09)	2.1729 (0.07)	2.1260 (0.08)	2.0851 (0.08)	2.0489 (0.08)	2.0162 (0.07)	800
	K-TRPDs	2.6906 (2.40)	2.4976 (1.51)	2.3798 (0.10)	2.2947 (0.09)	2.2280 (0.09)	2.1729 (0.07)	2.1260 (0.08)	2.0851 (0.08)	2.0489 (0.08)	2.0162 (0.07)	**380**

then transformed into a two-rod structure as shown in figure 6. As a result of corrosion, both the inner and outer diameters will evolve over time [1]:

$$d(t) = d_0 + 2 \times 0.0008t \tag{64}$$

$$D(t) = D_0 - 2 \times 0.0008t, \tag{65}$$

where d_0 and D_0 denote initial values of $d(t)$ and $D(t)$, respectively; $P(t)$ stands for a stochastic process. The distributive stats are tabulated in table 3.

In this case, failure of the structural system occurs only when both the three-bar and two-bar structures fail, indicating that the system function is a parallel structure. Accordingly, the failure modes of the three-bar structure and the two-bar structure can be established as [1]

$$g_1(t) = \eta - \frac{4P(t)L^3}{\pi\left(L^3 + 2H^3\right)\left(D(t)^2 - d(t)^2\right)} \tag{66}$$

$$g_2(t) = \eta - \frac{2P(t)L}{\pi H\left(D(t)^2 - d(t)^2\right)}. \tag{67}$$

Five discrete time step lengths (Cases 1–5) are examined. Time steps for these five cases are set to 1/2 year, 2/5 year, 1/3 year, 1/4 year, and 1/5 year, respectively. For each case, MCS with 10^6 random samples and the TRPD and K-TRPD methods are applied. The corresponding results are tabulated in table 4 and depicted in figure 7. The results from TRPDs and K-TRPDS are benchmarked against the results from MCS.

Table 4 demonstrates that as the discrete time step decreases, the results from TRPDs and K-TRPDs converge towards those from the MCS method. In Case 5, the maximum relative deviation between the results of the two methods from that by MSC is 2.75% and 2.74%, respectively, demonstrating the high accuracy of the K-TRPD method. In Case 5, the $t = 10$, $g_1(t)$ and $g_2(t)$ reliability indexes are 1.4503 and 0.9991. The system reliability index considering the parallel failure mode is 2.0162, which is higher than the counterpart for the single failure mode. This conforms to general engineering practice. For computational efficiency, as the discrete time step increases, the number of function calls for TRPDs increases substantially, whereas the increase for K-TRPDs is limited to just 420 calls. In Case 5, the TRPD method entails notably more function calls than K-TRPDs, signifying the improved computational efficiency due to the engagement of the Kriging model in K-TRPDs.

4.3. Two-bar parallel structure

Figure 8 shows a parallel structure of two rods. A-A and B-B are the cross-sections of rod 1 and rod 2, respectively. Considering that materials degrade over time, the lengths and widths of the two rod sections are expressed as

$$a_1(t) = a_0^1 - 2k_1t \tag{68}$$

$$a_2(t) = a_0^2 - 2k_2t \tag{69}$$

$$b_1(t) = b_0^1 - 2k_1t \tag{70}$$

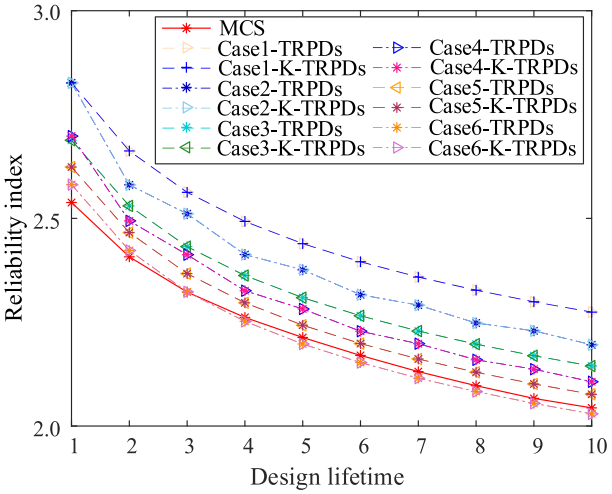

(a) Reliability index over design lifetime

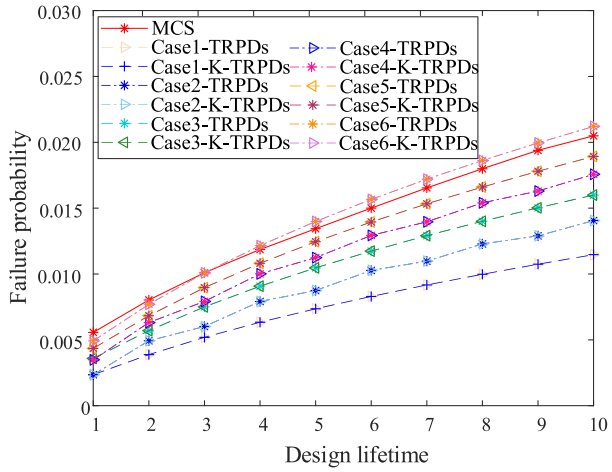

(b) Failure probability over design lifetime

Figure 4. Two indexes for simply supported beam over design lifetime.

$$b_2(t) = b_0^2 - 2k_2 t, \tag{71}$$

where $a_1(t)$, $a_2(t)$ and $b_1(t)$, $b_2(t)$ are the widths and lengths of the two cross sections, respectively; a_0^1, a_0^2, b_0^1 and b_0^2 are the initial values of $a_1(t)$, $a_2(t)$, $b_1(t)$ and $b_2(t)$, respectively; $k_1 = 5 \times 10^{-4}$, and $k_2 = 3 \times 10^{-4}$.

When the yield strength of both bars is lower than the applied stress, the entire structural system will fail, indicating that this system operates as a parallel system. The performance function for this two-bar parallel structure can be expressed as

$$g(t) = \begin{cases} G_1(t) = a_1(t) b_1(t) \sigma_1 - P(t)/2 \\ G_2(t) = a_2(t) b_2(t) \sigma_2 - P(t)/2 \end{cases}, \tag{72}$$

where σ_1 and σ_2 denote the respective yield strengths. Table 5 tabulates the distributive stats of each random variable. The time-variant reliability index is expressed as

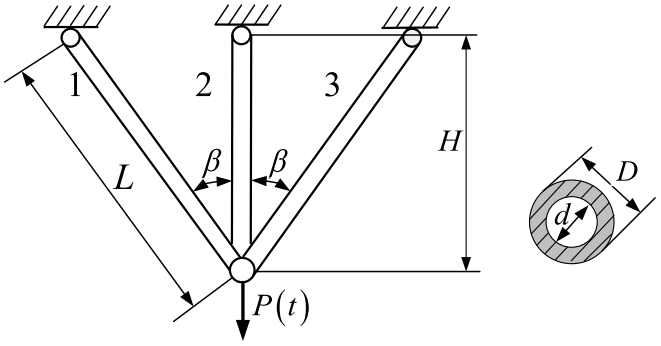

Figure 5. Planar three-bar structure [1].

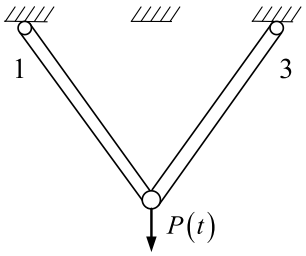

Figure 6. Planar two-bar structure [1].

Table 3. Distributive stats of random variables for a planar three-bar structure.

Variables	Distribution	Mean	COV (%)	Acf.
η	Normal	8 MPa	13	NA
D_0	Lognormal	0.05 m	16	NA
d_0	Lognormal	0.02 m	10	NA
L	Normal	1.5 m	26.7	NA
H	Normal	1 m	40	NA
$F(t)$	Gaussian process	3500 N	20	$\frac{\sin(\|\|8\tau\|\|)}{\|\|8\tau\|\|}$ [37]

$$P_s(t) = P\{g(\mathbf{X}, Y(t), t) \geq 0, \forall t \in [0,2]\}, \tag{73}$$

where $\mathbf{X} = \left[a_0^1, a_0^2, b_0^1, b_0^2, \sigma_1, \sigma_2\right]$ and $Y(t) = P(t)$.

Five distinct scenarios, labeled as Cases 1–5, are examined. The time steps are set to be 1/3 year, 1/5 year, 1/6 year, 1/10 year, and 1/14 year. For each case, this problem is solved using MCS with 10^7 samples. The results are presented in table 6.

Table 6 shows that as the discrete time step decreases, the results for TRPDs and K-TRPDs gradually converge to those by MCS method. When $t = 2$, the reliability indexes of $G_1(t)$ and $G_2(t)$ are 2.3026 and 2.2809 in Case 5, while the system reliability indexes of the parallel system are 2.6398. This is higher than the counterparts of the single failure mode, which conforms to general engineering practice. For computational efficiency, as the discrete time step increases from Case 1 to Case 5, the number of TRPD function calls increases from 432 to 2016, while the number of K-TRPD function calls increases from 312 to 664. A highlight is that for K-TRPDs, the increase

Table 4. Reliability index for the planar three-bar structure.

Cases	Time/year	1	2	3	4	5	6	7	8	9	10	NoF
	MCS	2.0385	1.9248	1.8609	1.8123	1.7606	1.7206	1.6830	1.6460	1.6164	1.5829	10^6
Case 1 (%)	TRPDs	2.2000 (7.92)	2.0618 (7.12)	1.9791 (6.35)	1.9170 (5.78)	1.8654 (5.95)	1.8196 (5.75)	1.7776 (5.62)	1.7380 (5.56)	1.7000 (5.17)	1.6632 (5.07)	14 320
	K-TRPDs	2.1998 (7.91)	2.0614 (7.10)	1.9782 (6.30)	1.9156 (5.70)	1.8640 (5.87)	1.8183 (5.68)	1.7760 (5.53)	1.7363 (5.49)	1.6986 (5.08)	1.6620 (5.00)	**3000**
Case 2 (%)	TRPDs	2.2122 (8.53)	2.0292 (5.43)	1.9619 (5.43)	1.8866 (4.10)	1.8453 (4.81)	1.7905 (4.06)	1.7570 (4.40)	1.7097 (3.87)	1.6795 (3.90)	1.6355 (3.32)	17 896
	K-TRPDs	2.2121 (8.52)	2.0287 (5.40)	1.9610 (5.38)	1.8852 (4.02)	1.8438 (4.72)	1.7891 (3.98)	1.7554 (4.31)	1.7081 (3.77)	1.6780 (3.81)	1.6344 (3.25)	**3070**
Case 3 (%)	TRPDs	2.1414 (5.05)	2.0086 (4.36)	1.9283 (3.62)	1.8677 (3.06)	1.8171 (3.21)	1.7722 (3.00)	1.7308 (2.84)	1.6918 (2.78)	1.6543 (2.34)	1.6178 (2.21)	21 481
	K-TRPDs	2.1413 (5.04)	2.0081 (4.33)	1.9273 (3.57)	1.8663 (2.98)	1.8157 (3.13)	1.7708 (2.92)	1.7292 (2.75)	1.6901 (2.68)	1.6529 (2.25)	1.6167 (2.14)	**3140**
Case 4 (%)	TRPDs	2.1134 (3.67)	1.9823 (2.99)	1.9022 (2.22)	1.8417 (1.62)	1.7912 (1.74)	1.7464 (1.50)	1.7051 (1.32)	1.6662 (1.23)	1.6288 (0.77)	1.5926 (0.61)	28 640
	K-TRPDs	2.1133 (3.67)	1.9818 (2.97)	1.9012 (2.17)	1.8403 (1.54)	1.7898 (1.66)	1.7450 (1.42)	1.7035 (1.22)	1.6645 (1.12)	1.6274 (0.68)	1.5914 (0.54)	**3280**
Case 5 (%)	TRPDs	2.0945 (2.75)	1.9635 (2.01)	1.8832 (1.20)	1.8226 (0.57)	1.7720 (0.65)	1.7272 (0.38)	1.6860 (0.18)	1.6471 (0.07)	1.6099 (0.41)	1.5737 (0.59)	35 832
	K-TRPDs	2.0943 (2.74)	1.9630 (1.99)	1.8822 (1.14)	1.8211 (0.49)	1.7706 (0.57)	1.7258 (0.30)	1.6843 (0.08)	1.6454 (0.03)	1.6084 (0.50)	1.5725 (0.66)	**3420**

is as low as 352 against a 1574 increase for TRPDs, signifying the enhanced computational efficiency of K-TRPDs.

4.4. RV reducer

RV reducers are generally employed in robots, due to favorable features of compacted size, lightweight, and high output torque. Any form of failure in the RV reducer will impact the overall reliability of the robot. Figure 9 is a schematic for an industrial robot and its RV reducer [49, 50]. In this example, considering the two failure modes of planetary gear tooth surface contact fatigue failure and bending fatigue failure of RV reducer, the performance functions $g_1(t)$ and $g_2(t)$ for tooth surface contact fatigue strength and bending fatigue strength of planetary gear teeth are formulated based on the condition criteria for the surface stress of the gears:

$$g_1(t) = [\sigma_{\mathrm{H}}] - \sqrt{\frac{2K_{\mathrm{H}}T}{b_2 d_2} \cdot \frac{\mu+1}{\mu}} Z_H Z_E Z_\varepsilon \tag{74}$$

$$g_2(t) = [\sigma_{\mathrm{F}}] - \frac{2K_{\mathrm{F}}TY_{\mathrm{Fa}}Y_{\mathrm{Sa}}Y_\varepsilon}{b_2 d_2 m}, \tag{75}$$

where $[\sigma_{\mathrm{H}}]$ and $[\sigma_{\mathrm{F}}]$ represent the allowable contact and bending fatigue strengths, respectively; K_{H} and K_{F} are the load coefficients to calculate these strengths; Z_H stands for the node area coefficient; Z_E denotes the elastic modulus; Z_ε specifies the coincidence coefficient for contact fatigue strength; Y_{Fa} refers the tooth shape coefficient; Y_{Sa} symbolizes the stress correction coefficient for the load acting on the tooth tip; Y_ε is the coincidence coefficient used in bending fatigue strength calculations; m indicates the modulus of the planetary gear; and μ is the ratio of the number of teeth on the planetary gear to those on the central gear. The distributive stats are tabulated in table 7.

Four distinct cases are analyzed, with time steps being set to 1 year, 5/6 year, 5/7 year and 5/8 year, respectively. MCS with 10^6 samples, TRPDs and K-TRPDs are applied to solve each case, and the results are presented in table 8. The variations of the reliability index and failure probability over the design lifetime are depicted in figure 10.

As the time step decreases, the results from the TRPD and K-TRPD methods converge towards those from the MCS method. Specifically, in Case 4, the maximum relative error between the results by the two methods is 4.92%, with K-TRPDs demonstrating a relatively higher level of accuracy. When considering the single failure mode, in Case 4, $t = 5$, $g_1(t)$ and $g_2(t)$ are 1.8199 and 5.2276, while the system reliability index considering the series of the two is 1.8198. This is lower than that of the single failure mode, which conforms to general engineering practice. For computational efficiency, the number of function calls in TRPDs increases significantly as the number of discretizations increases. For Cases 1–5, the function calls for TRPDs method increases by a factor of 180; whereas for the K-TRPD method, this increase is only 24 times. In Case 5, the number of functions calls for TRPD method is approximately double that of the K-TRPD method. This comparison signifies that integrating the

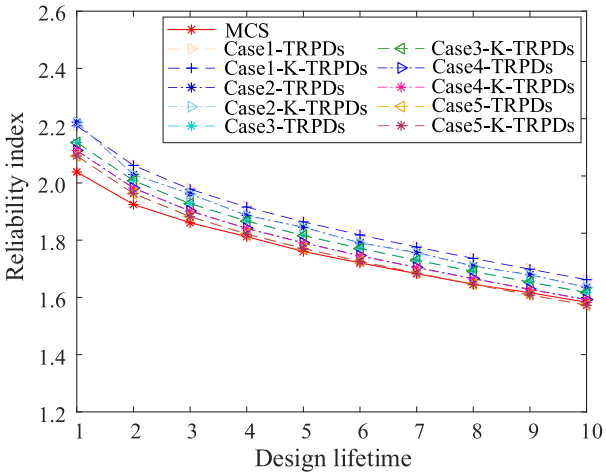

(a) Reliability index over design lifetime

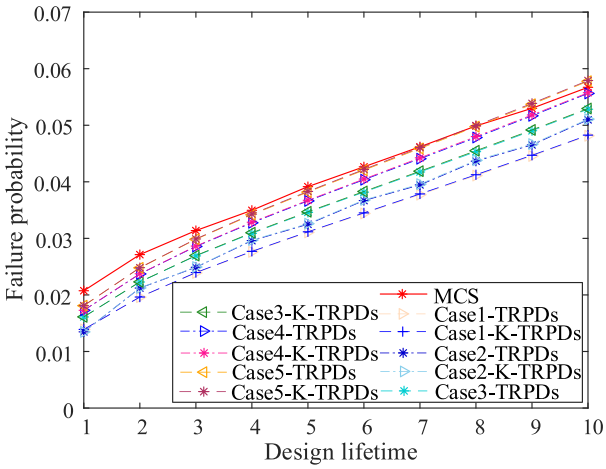

(b) Failure probability over design lifetime

Figure 7. Two indexes for planar three-bar structure over the design lifetime.

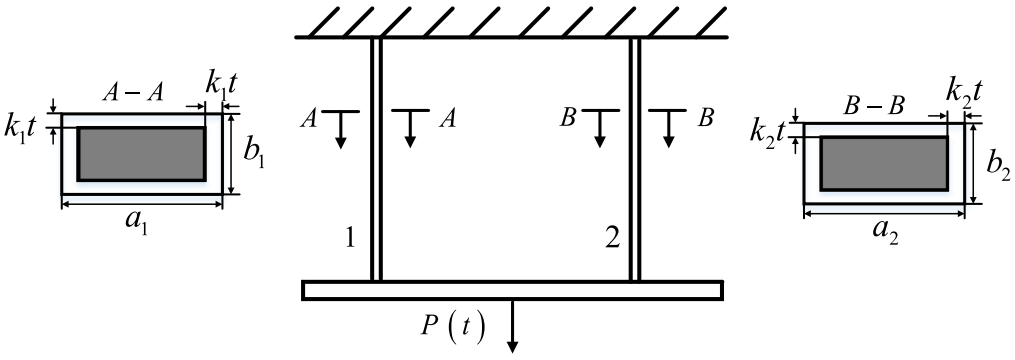

Figure 8. Two-bar parallel structure [1, 48].

K-TRPDs method with the Kriging model enhances computational efficiency compared to TRPD method alone.

4.5. Hybrid system example

The structural system consists of three components, A, B and C, with their interconnections being illustrated in figure 11. The performance functions for each unit are defined as follows,

$$A: g_1 = \frac{X_1^2}{5} + \frac{X_2}{2}(1 - 0.001t) - X_2 Y_1(t) - Y_2(t) \quad (76)$$

$$B: g_2 = 3X_1 + 2X_2^2 \exp(-0.001t) - X_1 Y_1(t) - X_1 Y_2(t) \quad (77)$$

Table 5. Distributive stats of random variables for a planar three-bar structure.

Variables	Distribution	Mean	COV (%)	Acf.
a_0^1	Normal	1.3 inch	0.8	NA
a_0^2	Normal	1.2 inch	0.8	NA
b_0^1	Normal	1.3 inch	3.8	NA
b_0^2	Normal	1.2 inch	4.2	NA
σ_1	Normal	34.1 kpsi	1.0	NA
σ_2	Normal	34.1 kpsi	1.0	NA
$P(t)$	Gaussian process	85 kpsi	9.4	$\exp\left[-(2\tau)^2\right]$

Table 6. Distributive stats of random variables for a planar three-bar structure.

Cases	Time/year	1	2	NoF
	MCS	2.8335	2.6292	10^7
Case 1 (%)	TRPDs	3.4911(23.21)	3.1563(20.05)	432
	K-TRPDs	3.4911(23.21)	3.1563(20.05)	**312**
Case 2 (%)	TRPDs	3.3130(16.92)	2.9738(13.01)	720
	K-TRPDs	3.3130(16.92)	2.9738(13.01)	**376**
Case 3 (%)	TRPDs	3.2524(14.78)	2.9113(10.73)	864
	K-TRPDs	3.2524(14.78)	2.9113(10.73)	**408**
Case 4 (%)	TRPDs	3.0906(9.07)	2.7438(4.36)	1440
	K-TRPDs	3.0906(9.07)	2.7438(4.36)	**536**
Case 5 (%)	TRPDs	2.9905(5.54)	2.6398(0.40)	2016
	K-TRPDs	2.9905(5.54)	2.6398(0.40)	**664**

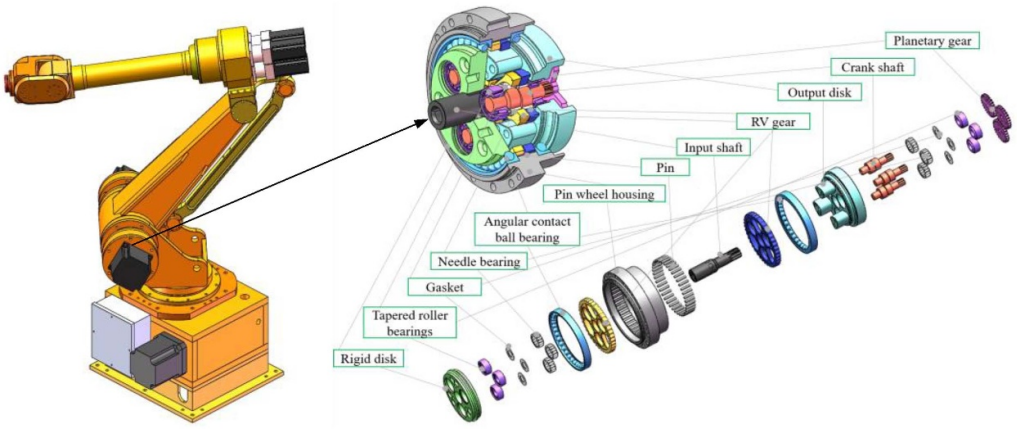

Figure 9. Schematic of an industrial robot and RV reducer [49, 50].

Table 7. Distributive stats of random variables for RV reducer.

Variables	Distribution	Mean	COV (%)	Acf.
d_2	Normal	20.5	0.01	NA
b_2	Normal	3.90	0.015	NA
$T(t)$	Gaussian process	1686	7	$\exp\left[-(0.1\tau)^2\right]$

Table 8. Reliability indexes for an industrial robot and RV reducer.

Cases	Time/year	1	2	3	4	5	NoF
	MCS	2.3523	2.2188	2.0825	1.9415	1.8005	10^6
Case 1 (%)	TRPDs	2.4554 (4.38)	2.2386 (0.89)	2.1035 (1.01)	1.9991 (2.97)	1.9095 (6.05)	300
	K-TRPDs	2.4553 (4.38)	2.2385 (0.89)	2.1034 (1.01)	1.9990 (2.96)	1.9094 (6.05)	**220**
Case 2 (%)	TRPDs	2.461 (4.62)	2.2506 (1.43)	2.1226 (1.93)	2.0261 (4.36)	1.8732 (4.03)	360
	K-TRPDs	2.461 (4.62)	2.2505 (1.43)	2.1225 (1.92)	2.0260 (4.35)	1.8731 (4.03)	**228**
Case 3 (%)	TRPDs	2.4650 (4.79)	2.2591 (1.82)	2.0447 (1.82)	1.9698 (1.46)	1.8440 (2.42)	420
	K-TRPDs	2.4650 (4.79)	2.2590 (1.81)	2.0447 (1.81)	1.9697 (1.45)	1.8439 (2.41)	**236**
Case 4 (%)	TRPDs	2.4680 (4.92)	2.1457 (3.29)	2.0584 (1.16)	1.9265 (0.77)	1.8199 (1.08)	480
	K-TRPDs	2.4680 (4.92)	2.1456 (3.30)	2.0583 (1.16)	1.9264 (0.78)	1.8198 (1.07)	**244**

$$C: g_3 = 4X_2 - \frac{X_2 Y_1(t)}{4} - \frac{X_1 Y_2(t)}{2} - 0.0002t. \tag{78}$$

Considering the time interval of $t = [0, 10]$, the structural reliability of the hybrid system can be written as

$$\begin{cases} A: \left\{ \forall t \in [0,T] \,|\, g_1 = \dfrac{X_1^2}{5} + \dfrac{X_2}{2}(1 - 0.001t) - X_2 Y_1(t) - Y_2(t) > 0 \right\} \\ B: \left\{ \forall t \in [0,T] \,|\, g_2 = 3X_1 + 2X_2^2 \exp(-0.001t) - X_1 Y_1(t) - X_1 Y_2(t) > 0 \right\}, \\ C: \left\{ \forall t \in [0,T] \,|\, g_3 = 4X_2 - \dfrac{X_2 Y_1(t)}{4} - \dfrac{X_1 Y_2(t)}{2} - 0.0002t > 0 \right\} \end{cases} \tag{79}$$

where g_1, g_2 and g_3 are the three functional functions of structural units *A, B* and *C*, respectively. The relationships among *A, B* and *C* are illustrated in figure 11, in which *A* is parallel to *B* and *C*. The reliability index is expressed as

$$P_s(T) = \mathrm{Prob}\{A \cup [B \cap C]\}. \tag{80}$$

For this structural system, X_1 and X_2 denote random variables and $Y_1(t)$ and $Y_2(t)$ represent Gaussian processes. The distributive stats of the variables and processes are tabulated in table 9.

In this example, the system is a hybrid time-variant reliability model involving two stochastic processes. Six different cases (Cases 1–6) are considered, with time steps being set at 1 year, 2/3 year, 1/2 year, 2/5 year, 1/3 year, and 1/4 year, respectively. For each case, MCS, TRPD, and K-TRPD methods are employed to solve the problem. The results are presented in table 9. The variations of the reliability index and failure probability over time are depicted in figure 12.

Table 10 suggests that when MCS is applied, the number of random samples used for analysis is comparable with those of the TRPD and K-TRPD methods. As illustrated in figure 12, as the time step decreases, the results from the TRPD and K-TRPD methods converge towards those from the MCS method. For large time steps, such as in Case 6, the maximum deviation between the two methods is as low as 1.70%, both aligning closely with MCS results. For computational efficiency, table 10 indicates that for the different time steps in Cases 1–6, the number of functions calls for TRPDs are 1260, 1890, 2520, 3150, 3780 and 5040 times, and 528, 603, 678, 753, 828 and 978 times for K-TRPDs, respectively. As the discrete number increases, the TRPD method exhibits a more significant increase in the number of function calls. Specifically, from Case 1 to Case 6, the function calls for TRPDs increases by 3780 times, whereas for K-TRPDs, the increase is only 450 times. In Case 6, the number of functions calls for TRPD method is approximately five times that of the K-TRPD method. This analysis demonstrates that K-TRPD

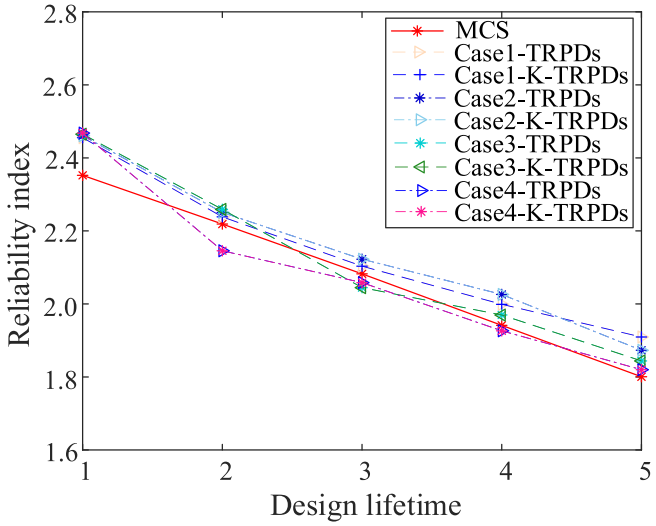

(a) Reliability index over design lifetime

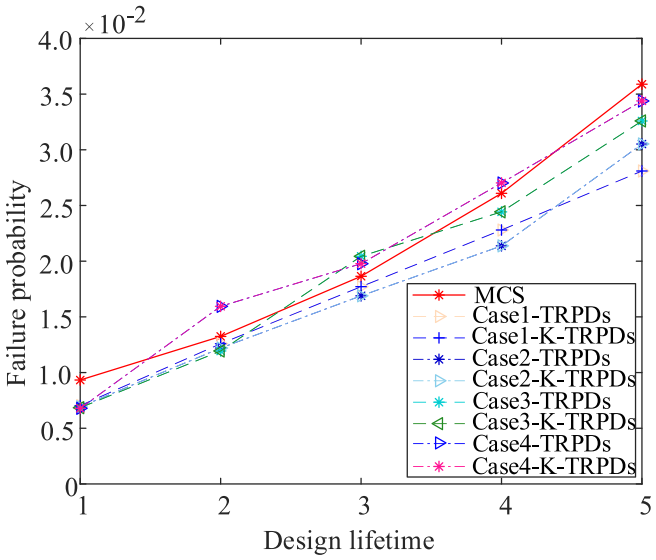

(b) Failure probability over design lifetime

Figure 10. Two indexes for an RV reducer over the design lifetime.

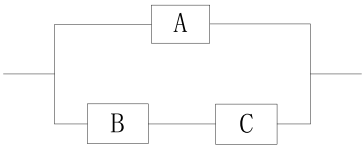

Figure 11. Hybrid structure.

Table 9. Distributive stats of random variables in a mixed-link structural system [37].

Variables	Distribution	Mean	COV (%)	Acf.
X_1	Lognormal	6	10	NA
X_2	Lognormal	5	10	NA
$Y_1(t)$	Gaussian process	4	10	$\exp\left(-2\tau^2\right)$
$Y_2(t)$	Gaussian process	3	10	$\frac{\sin(\|\|2\tau\|\|)}{\|\|2\tau\|\|}$

Table 10. Reliability index for a mixed-link structural system.

Cases	Time/year	1	2	3	4	5	6	7	8	9	10	NoF
	MCS	2.5383	2.4075	2.3226	2.2616	2.2133	2.1701	2.1311	2.0972	2.0665	2.0437	10^6
Case 1 (%)	TRPDs	2.8260 (11.33)	2.6624 (10.59)	2.5629 (10.35)	2.4927 (10.22)	2.4393 (10.21)	2.3956 (10.39)	2.3588 (10.68)	2.3271 (10.96)	2.2993 (11.27)	2.2743 (11.28)	1260
	K-TRPDs	2.8260 (11.33)	2.6624 (10.59)	2.5629 (10.35)	2.4927 (10.22)	2.4393 (10.21)	2.3956 (10.39)	2.3588 (10.68)	2.3271 (10.96)	2.2993 (11.27)	2.2744 (11.29)	**528**
Case 2 (%)	TRPDs	2.8265 (11.35)	2.5808 (7.20)	2.5111 (8.12)	2.4129 (6.69)	2.3762 (7.36)	2.3163 (6.74)	2.2912 (7.51)	2.2481 (7.20)	2.2293 (7.88)	2.1957 (7.44)	1890
	K-TRPDs	2.8265 (11.35)	2.5808 (7.20)	2.5111 (8.12)	2.4129 (6.69)	2.3762 (7.36)	2.3163 (6.74)	2.2912 (7.51)	2.2481 (7.20)	2.2293 (7.88)	2.1957 (7.44)	**603**
Case 3 (%)	TRPDs	2.6882 (5.91)	2.5302 (5.10)	2.4320 (4.71)	2.3625 (4.46)	2.3092 (4.33)	2.2655 (4.40)	2.2288 (4.58)	2.1972 (4.77)	2.1694 (4.98)	2.1446 (4.94)	2520
	K-TRPDs	2.6882 (5.91)	2.5302 (5.10)	2.4320 (4.71)	2.3625 (4.46)	2.3092 (4.33)	2.2655 (4.40)	2.2288 (4.58)	2.1972 (4.77)	2.1694 (4.98)	2.1446 (4.94)	**678**
Case 4 (%)	TRPDs	2.6982 (6.30)	2.4941 (3.60)	2.4126 (3.87)	2.3259 (2.84)	2.2820 (3.10)	2.2283 (2.68)	2.1983 (3.15)	2.1596 (2.98)	2.1370 (3.41)	2.1067 (3.08)	3150
	K-TRPDs	2.6982 (6.30)	2.4941 (3.60)	2.4126 (3.87)	2.3259 (2.84)	2.2820 (3.10)	2.2283 (2.68)	2.1983 (3.15)	2.1596 (2.98)	2.1370 (3.41)	2.1067 (3.08)	**753**
Case 5 (%)	TRPDs	2.6236 (3.36)	2.4658 (2.42)	2.3671 (1.92)	2.2968 (1.56)	2.2428 (1.33)	2.1987 (1.32)	2.1615 (1.43)	2.1296 (1.54)	2.1015 (1.69)	2.0764 (1.60)	3780
	K-TRPDs	2.6236 (3.36)	2.4658 (2.42)	2.3670 (1.91)	2.2968 (1.56)	2.2428 (1.33)	2.1987 (1.32)	2.1615 (1.43)	2.1296 (1.54)	2.1015 (1.69)	2.0764 (1.60)	**828**
Case 6 (%)	TRPDs	2.5814 (1.70)	2.4227 (0.63)	2.3231 (0.02)	2.2522 (0.42)	2.1976 (0.71)	2.1529 (0.79)	2.1153 (0.74)	2.0831 (0.67)	2.0547 (0.57)	2.0295 (0.69)	5040
	K-TRPDs	2.5814 (1.70)	2.4227 (0.63)	2.3231 (0.02)	2.2522 (0.42)	2.1976 (0.71)	2.1529 (0.79)	2.1153 (0.74)	2.0831 (0.67)	2.0547 (0.57)	2.0295 (0.69)	**978**

method, when integrated with the Kriging model, achieves improved computational efficiency compared to the TRPD method.

5. Conclusions

The stochastic process discretization of TRPDs is similar to MCS in that accuracy increases with the increasing number of discrete moments. However, as the number of discrete stochastic processes and time intervals increase, the computational time increases exponentially. As a result, the number of discretized stochastic processes has to be kept low, which is susceptible to instability in reliability results. This study introduces a novel method for analyzing the reliability of time-variant systems with multiple failure modes using the Kriging model. Initially, the reliability analysis for various types of time-variant systems is converted into a series of single-failure-mode time-variant reliability problems. The stochastic process is then discretized to create a set of time-invariant problems. Discrete moments are selected to solve the MPP and build a Kriging model. To enhance computational efficiency, an active learning function is incorporated. The constructed Kriging model is then used to predict the MPP trajectory for each failure mode, ultimately yielding reliability for the time-varying system.

The currently proposed K-TRPD method not only significantly reduces the computational cost of TRPDs by introducing an active learning Kriging model to select some of the points that have the greatest impact on the model accuracy, but also allows for prediction of more unknown MPP points, thereby enhancing the stability of reliability and improving computational accuracy. Tests are conducted on three different systems including series, parallel, and hybrid systems to verify the

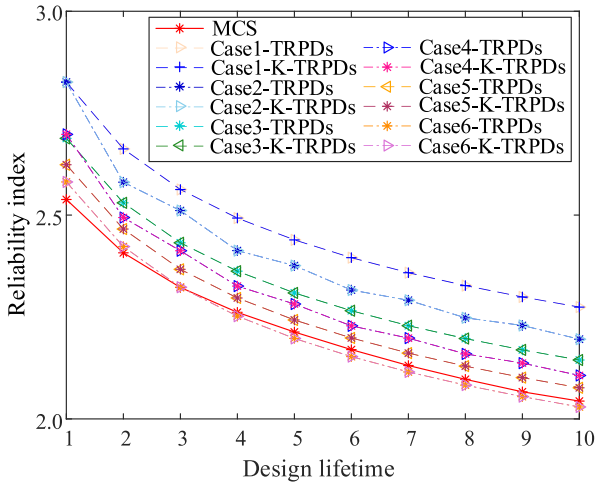

(a) Reliability index over design lifetime

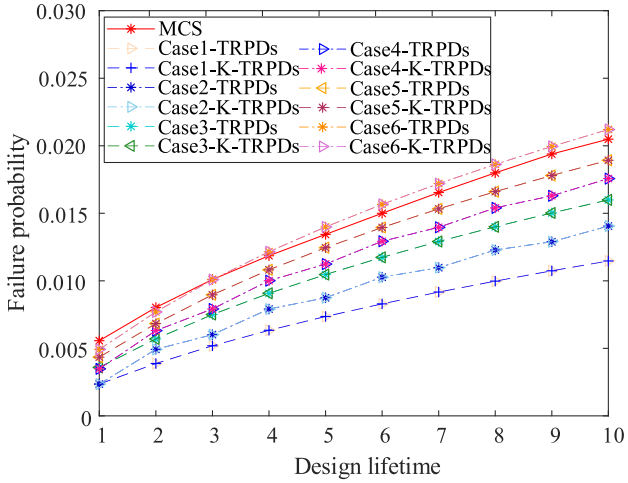

(b) Failure probability over design lifetime

Figure 12. Two indexes for a hybrid structural system over the design lifetime.

proficiency of the currently proposed method. Comparisons of results demonstrate that the currently proposed method is a highly promising alternative for analyzing the reliability of time-varying systems.

A note of attention is that the currently proposed method does not account for the potential complex correlation among different failure modes. In practical structural systems, different components may be subjected to common loads, dimensional parameters, and materials, which gives rise to correlations between different failure modes. These correlations may impact the results of structural reliability analysis, highlighting an important direction for our future efforts..

Acknowledgments

The authors would like to acknowledge the financial supports from the National Science Foundation for Excellent Young Scholars (Grant No. 52422507), the National Natural Science Foundation of China (Grant No. 52275244) and the Cross-Disciplinary Graduate Program of HEBUT (Grant No. XKJC-2023014).

Conflict of interest

The authors declare that they have no conflict of interest.

References

[1] Jiang C, Wei X, Huang Z and Liu J 2017 An outcrossing rate model and its efficient calculation for time-dependent system reliability analysis *ASME-J. Mech. Des.* **139** 041402

[2] Zhou F, Hou Y and Nie H 2022 On high-dimensional time-variant reliability analysis with the maximum entropy principle *Int. J. Aerosp. Eng.* **2022** 6612864

[3] Zhao Y, Zhang D, Yang M, Wang F and Han X 2024 On efficient time-dependent reliability analysis method through most probable point-oriented Kriging model combined with importance sampling *Struct. Multidiscip. Optim.* **67** 6
[4] Jiang C, Qiu H, Gao L, Wang D, Yang Z and Chen L 2020 Real-time estimation error-guided active learning Kriging method for time-dependent reliability analysis *Appl. Math. Modell.* **77** 82–98
[5] Andrieu-Renaud C, Sudret B and Lemaire M 2004 The PHI2 method: a way to compute time-variant reliability *Reliab. Eng. Syst. Saf.* **84** 75–86
[6] Coleman J 1959 Reliability of aircraft structures in resisting chance failure *Oper. Res.* **7** 639–45
[7] Siegert A 1951 On the first passage time probability problem *Phys. Rev.* **81** 617–23
[8] Wen Y 1976 Method for random vibration of hysteretic system *J. Eng. Mech. Div.* **102** 249–63
[9] Rice S 1944 Mathematical analysis of random noise *Bell Syst. Tech. J.* **23** 282–332
[10] Rice S 1945 Mathematical analysis of random noise *Bell Syst. Tech. J.* **24** 46–156
[11] Engelund S, Rackwitz R and Lange C 1995 Approximations of first-passage times for differentiable processes based on higher-order threshold crossings *Probab. Eng. Mech.* **10** 53–60
[12] Schall G, Faber M H and Rackwitz R 1991 The ergodicity assumption for sea states in the reliability estimation of offshore structures *J. Offshore Mech. Arct. Eng.* **113** 241–6
[13] Rackwitz R 1998 Computational techniques in stationary and non-stationary load combination—A review and some extensions *J. Struct. Eng.* **25** 1–20
[14] Zhang J and Du X 2011 Time-dependent reliability analysis for function generator mechanisms *ASME-J. Mech. Des.* **133** 031005
[15] Yang M, Zhang D and Han X 2020 New efficient and robust method for structural reliability analysis and its application in reliability-based design optimization *Comput. Methods Appl. Mech. Eng.* **366** 113018
[16] Sudret B 2008 Analytical derivation of the outcrossing rate in time-variant reliability problems *Struct. Infrastruct. Eng.* **4** 353–62
[17] Singh A, Mourelatos Z P and Li J 2009 Design for lifecycle cost using time-dependent reliability *ASME 2009 Int. Design Engineering Technical Conf. and Computers and Information in Engineering Conf.* pp 1105–19
[18] Singh A, Mourelatos Z P and Nikolaidis E 2011 An importance sampling approach for time-dependent reliability *ASME 2011 Int. Design Engineering Technical Conf. and Computers and Information in Engineering Conf.* pp 1077–88
[19] Hu Z, Li H, Du X and Chandrashekhara K 2013 Simulation-based time-dependent reliability analysis for composite hydrokinetic turbine blades *Struct. Multidiscip. Optim.* **47** 765–81
[20] Jiang C, Huang X, Han X and Zhang D Q 2014 A time-variant reliability analysis method based on stochastic process discretization *ASME-J. Mech. Des.* **136** 091009
[21] Jiang C, Wei X, Wu B and Huang Z L 2018 An improved TRPD method for time-variant reliability analysis *Struct. Multidiscip. Optim.* **58** 1935–46
[22] Zhang D, Zhou P, Jiang C, Yang M, Han X and Li Q 2021 A stochastic process discretization method combing active learning Kriging model for efficient time-variant reliability analysis *Comput. Methods Appl. Mech. Eng.* **384** 113990
[23] Yuan X, Shu Y, Qian Y and Dong Y 2024 Adaptive importance sampling approach for structural time-variant reliability analysis *Struct. Multidiscip. Optim.* **111** 102500
[24] Song Z, Zhang H, Zhang L, Liu Z and Zhu P 2022 An estimation variance reduction-guided adaptive Kriging method for efficient time-variant structural reliability analysis *Mech. Syst. Signal Process.* **178** 109322
[25] Wu J, Jiang Z, Song H, Wan L and Huang F 2021 Parallel efficient global optimization method: a novel approach for time-dependent reliability analysis and applications *Expert Syst. Appl.* **184** 115494
[26] Ji Y, Liu H, Xiao N and Zhan H 2023 An efficient method for time-dependent reliability problems with high-dimensional outputs based on adaptive dimension reduction strategy and surrogate model *Eng. Struct.* **276** 115393
[27] Song Z, Zhang H, Zhai Q, Zhang B, Liu Z and Zhu P 2024 A dimension reduction-based Kriging modeling method for high-dimensional time-variant uncertainty propagation and global sensitivity analysis *Mech. Syst. Signal Process.* **219** 111607
[28] Guo H, Dong Y and Gardoni P 2023 Adaptive subset simulation for time-dependent small failure probability incorporating first failure time and single-loop surrogate model *Struct. Saf.* **102** 102327
[29] Hagen Ø and Tvedt L 1991 Vector process out-crossing as parallel system sensitivity measure *J. Eng. Mech.* **117** 2201–20
[30] Dey A and Mahadevan S 2000 Reliability estimation with time-variant loads and resistances *J. Struct. Eng.* **126** 612–20
[31] Son Y K and Savage G J 2007 Set theoretic formulation of performance reliability of multiple response time-variant systems due to degradations in system components *Qual. Reliab. Eng. Int.* **23** 171–88
[32] Burgazzi L 2008 About time-variant reliability analysis with reference to passive systems assessment *Reliab. Eng. Syst. Saf.* **93** 1682–8
[33] Gupta S, Van Gelder P and Pandey M 2006 Time-variant reliability analysis for series systems with log-normal vector response *Advances in Engineering Structures, Mechanics & Construction* pp 747–59
[34] Melchers R E and Beck A T 2018 *Structural Reliability Analysis and Prediction* (Wiley)
[35] Song J and Der Kiureghian A 2006 Joint first-passage probability and reliability of systems under stochastic excitation *J. Eng. Mech.* **132** 65–67
[36] Liu P and Kiureghian A 1986 Multivariate distribution models with prescribed marginals and covariances *Probab. Eng. Mech.* **1** 105–12
[37] Yuan K, Xiao N, Wang Z and Shang K 2019 System reliability analysis by combining structure function and active learning Kriging model *Reliab. Eng. Syst. Saf.* **195** 106734
[38] Awruch G 2004 Comparison of response surface and neural network with other methods for structural reliability analysis *Struct. Saf.* **26** 49–67
[39] Meng Y, Zhang D, Shi B, Wang D and Wang F 2024 An active learning Kriging model with approximating parallel strategy for structural reliability analysis *Reliab. Eng. Syst. Saf.* **247** 110098
[40] Zafar T, Yanwei Z and Wang Z 2020 An efficient Kriging based method for time-dependent reliability based robust design optimization via evolutionary algorithm *Comput. Methods Appl. Mech. Eng.* **372** 113386
[41] Li J and Chen J 2019 Solving time-variant reliability-based design optimization by PSO-t-IRS: a methodology incorporating a particle swarm optimization algorithm and

an enhanced instantaneous response surface *Reliab. Eng. Syst. Saf.* **191** 106580
[42] Yang M, Zhang H, Zhang D, Han X and Li Q 2024 Time-variant reliability-based robust optimization for structures with material degradation *Comput. Methods Appl. Mech. Eng.* **432** 117337
[43] Xiao N, Zhan H and Yuan K 2020 A new reliability method for small failure probability problems by combining the adaptive importance sampling and surrogate models *Comput. Methods Appl. Mech. Eng.* **372** 113336
[44] Qian H, Huang T and Huang H 2021 A single-loop strategy for time-variant system reliability analysis under multiple failure modes *Mech. Syst. Signal Process.* **148** 107159
[45] Wang D, Zhang D, Meng Y, Yang M, Meng C, Han X and Li Q 2023 AK-HR^{n}: an efficient adaptive Kriging-based n-hypersphere rings method for structural reliability analysis *Comput. Methods Appl. Mech. Eng.* **414** 116146
[46] Bichon B, Eldred M, Swiler L Mahadevan S and McFarland J M 2008 Efficient global reliability analysis for nonlinear implicit performance functions *AIAA J.* **46** 2459–68
[47] Yang X, Liu Y, Gao Y, Zhang Y and Gao Z 2014 An active learning Kriging model for hybrid reliability analysis with both random and interval variables *Struct. Multidiscip. Optim.* **51** 1003–16
[48] Hu Z and Mahadevan S 2015 Time-dependent system reliability analysis using random field discretization *ASME-J. Mech. Des.* **137** 101404
[49] Qian H, Huang H and Li Y 2019 A novel single-loop procedure for time-variant reliability analysis based on Kriging model *Appl. Math. Modell.* **75** 735–48
[50] Yang M, Zhang D, Cheng C and Han X 2021 Reliability-based design optimization for RV reducer with experimental constraint *Struct. Multidiscip. Optim.* **63** 2047–64

Dequan Zhang (born 1990) is a Professor of Mechanical Engineering, Hebei University of Technology, Tianjin, China. He received PhD in mechanical engineering from Hunan University, Hunan, China in 2018. His research interests include reliability analysis, design under uncertainty and robotics.

Hongfei Zhang (born 1998) received BEng in Mechanical Engineering from Hebei University of Technology in 2021. He is currently pursuing PhD in Mechanical Engineering with Hebei University of Technology, Tianjin, China. His research interests include time-variant reliability analysis and machine learning.

Pengfei Zhou (born 1995) received the MS in Mechanical Engineering from Hebei University of Technology, Tianjin, China in 2022. His research interests include time-variant reliability analysis and time-variant design optimization.

Xing-ao Li (born 1998) received BEng in Mechanical Engineering from Hebei University of Technology in 2020. He is currently pursuing PhD in Mechanical Engineering with Hebei University of Technology, Tianjin, China. His research interests include uncertainty analysis, Bayesian inference and reliability analysis.

Fang Wang (born 1965) is a Professor of Mechanical Engineering, Hebei University of Technology, Tianjin, China. Her research interests include robot reliability analysis and robot intelligent sensing.

Xu Han (born 1968) is currently a Professor in Simulation-Based Design Theory and Methods with the School of Mechanical Engineering, Hebei University of Technology, Tianjin, China. His research interests include simulation-based design theory and methods, inverse problem theory and method, uncertainty analysis and reliability-based design.